



UNIVERSITY OF NEW HAMPSHIRE

TECH 797: SENIOR DESIGN PROJECT

---

# VFG Support Structure

---

*Authors:*

Shane BAIA

Chris CARRIER

*Advisors:*

Dr. Kenneth BALDWIN

Dr. Martin WOSNIK

May 18, 2011

## Acknowledgements

This work is the result of research sponsored in part, by the National Sea Grant College Program, NOAA, Department of Commerce, under grant #NA06OAR4170109 through the New Hampshire Sea Grant College Program.

Our group would also like to thank the following people and groups:

- We would like to thank our two advisors, Dr. Kenneth Baldwin and Dr. Martin Wosnik for their leadership and guidance throughout the project.
- We would like to thank our graduate student, Matthew Rowell for giving us hours of his time to help us move and assemble our structure... we couldn't have done it without you.
- We thank Jennifer Bedsole for her organizational support
- We would like to thank both Bob Champlin and Paul Lavoie for the contribution of their knowledge and skills to the project, as well as Andy McLeod for allowing us to use space within Chase Hall.
- We would like to thank the following companies for their support:
  - Bicycle Bob's
  - Collins Sheet Metal Inc.
  - Custom Welding and Fabrication Inc.
  - Fastener Warehouse
  - Northeast Industrial Technologies
- Special Thanks to Northeast Industrial Technologies for the use of their facility, staff and equipment. They are the only reason the airfoils were able to be finished on schedule and on budget.
- We thanks The University of New Hampshire Departments of Ocean and Mechanical Engineering for the use of their facilities and necessary tools throughout the development of our project.

## Contents

<b>1</b>	<b>Background Information</b>	<b>4</b>
<b>2</b>	<b>Problem Statement/Goals</b>	<b>4</b>
<b>3</b>	<b>Design of Support Structure</b>	<b>5</b>
3.1	Previous Work . . . . .	5
3.2	Alternate Designs . . . . .	7
3.3	Static Analysis . . . . .	8
3.4	Stress Concentration . . . . .	9
<b>4</b>	<b>SolidWorks FEA Analysis</b>	<b>11</b>
4.1	Flow Simulations . . . . .	11
4.2	Displacement Analysis . . . . .	15
4.3	FEA Analysis . . . . .	17
<b>5</b>	<b>Connection Analysis</b>	<b>20</b>
5.1	Bolted Connections . . . . .	20
5.2	Welded Connections . . . . .	22
<b>6</b>	<b>Additional Analysis</b>	<b>25</b>
6.1	Buoyancy Calculations . . . . .	25
6.2	Measuring Rotational Speed of the Rotor . . . . .	26
<b>7</b>	<b>Final Design</b>	<b>29</b>
7.1	Testing Site . . . . .	29
7.2	Assembly . . . . .	29
7.3	Deployment Plan . . . . .	29
<b>8</b>	<b>Construction of Support Structure</b>	<b>31</b>
8.1	Airfoils . . . . .	31
8.2	Top Frame . . . . .	32
8.3	Box . . . . .	33
8.4	Mounting on Barge . . . . .	33
8.5	Cable/Flotation Setup . . . . .	34
8.6	Torque Measurement/Construction . . . . .	35
<b>9</b>	<b>Testing/Deployment</b>	<b>37</b>
9.1	Drag Testing . . . . .	37
9.2	First Turbine Deployment . . . . .	39
<b>10</b>	<b>Future Work and Recommendations for Future Experiments</b>	<b>42</b>
<b>11</b>	<b>Conclusion</b>	<b>42</b>
<b>12</b>	<b>Appendices</b>	<b>42</b>

## List of Figures

1	CAD model of old turbine testing structure mounted to UNH's barge . . . . .	5
2	Corrosion on old turbine test structure . . . . .	6
3	CAD model of UNH's first generation VFG turbine . . . . .	6
4	Several Design ideas that were never implemented . . . . .	7
5	Free body diagram of the front airfoil . . . . .	9
6	Free body diagram of the rear airfoils . . . . .	9
7	Stress element at stress concentration located at the end of the rear airfoil . . . . .	10
8	Pressure and Velocity cut plots for Flow Analysis over Square Bar Tubing . . . . .	13
9	Pressure and Velocity cut plots for Flow Analysis over Triangular Faced Tubing . . . . .	14
10	Pressure and Velocity cut plots for Flow Analysis over Ellipse Airfoil . . . . .	14
11	Cross Section of Beam Designs . . . . .	15
12	SolidWorks FEA Setup of Triangular Faced Beam . . . . .	16
13	Figure describing setup of assembly for FEA Analysis . . . . .	18
14	Progression of SolidWorks FEA Analysis Results on Assembly . . . . .	18
15	Free body diagram of the front airfoil connection to the mounting box . . . . .	20
16	Free body diagram of the rear airfoil connection to the mounting box . . . . .	21
17	Free body diagram of the rear airfoil connection to the top frame . . . . .	21
18	Free body diagram of the front airfoil connection to the top frame . . . . .	22
19	Free body diagram of the bolted connection holding the frame together . . . . .	22
20	Various parts of a Convex Fillet Weld . . . . .	23
21	Diagram of the front laser tachometer device test setup . . . . .	26
22	Plot comparing the accuracy of the laser tachometer at various distances . . . . .	27
23	Completed Tripod Assembly . . . . .	30
24	Hip-Towing the barge using the Galen J . . . . .	30
25	The three completed airfoil struts and two extra sections . . . . .	31
26	Water Jet machine and JIG for assembling airfoils . . . . .	32
27	Plate and Gussets attached to the airfoil . . . . .	32
28	Completed top frame assembly mounted on the barge . . . . .	33
29	Completed box assembly . . . . .	34
30	Flotation test of structure with simulated turbine weight . . . . .	36
31	Simple diagram of torque transducer to be applied to turbine . . . . .	36
32	Hip Tow setup with Galen J. boat and Force Transducer . . . . .	37
33	Initial drag data for both with and without the tripod attached . . . . .	38
34	Overall drag of the structure compared to speed . . . . .	38
35	Cycle of pictures showing deployment procedures as described above . . . . .	40
36	Image taken underwater of joint deployment . . . . .	41

## List of Tables

1	Forces acting on various positions . . . . .	9
2	Table of Dimensions for each Geometric Shape . . . . .	11
3	Table of Calculated Drag vs. SolidWorks Analysis . . . . .	12
4	Table of comparison between SolidWorks and Analytical deflection calculations . . . . .	17
5	End Results from Weld Calculations . . . . .	24
6	Buoyancy Calculations of each part of Tripod . . . . .	25
7	Comparing Laser Tachometer to Motor Tachometer . . . . .	26
8	Measuring Respective Transient Accuracy . . . . .	27
9	Laser Angle of Attack $0^\circ$ . . . . .	28
10	Laser Angle of Attack $15^\circ$ . . . . .	28
11	Laser Angle of Attack $45^\circ$ . . . . .	28

## 1 Background Information

In today's world, the crux of many engineering projects is the development of clean renewable energy sources. Of these sources, almost none are as enticing as the kinetic energy within our vast oceans and waterways. The tidal cycle of our oceans is caused by the gravitational forces of the Moon and Sun. The movement of the water during these daily cycles requires tremendous amounts of energy that can be extracted mechanically as a perfectly clean and renewable source. This can be done with many machines such as water mills, dams, and more recently the hydrokinetic turbine.

The hydrokinetic turbine works the same as a wind turbine except, with water being a thousand times as dense as air, it has the potential to harvest significantly larger amounts of energy. With the larger payoff, comes the difficulty in designing and deploying electrical/mechanical devices underwater. Because of this difficulty, this technology is relatively new and is far from perfected. Of the many hydrokinetic turbine designs, we will be testing one that features variable flux generation (VFG). VFG is a mechanism that is designed to increase the efficiency of the turbine by reducing the required startup torque to spin the turbine. Research into this design has been done in the past, but we hope to further this research by testing UNH's second generation VFG turbine in a more realistic environment such as the Ocean.

## 2 Problem Statement/Goals

The Turbine Deployment Structure is part of a joint venture to build and test the second generation Hydrokinetic Turbine featuring Variable Flux Generation (VFG). The motive behind building this test structure was to provide the turbine production team a platform to definitively test the VFG Turbine concept in a real-world ocean environment. Unlike past test structures, ours was designed to sustain larger horizontal axis turbines than can be tested in the tow tanks at the ocean engineering facility in Chase Hall. It was also designed to allow a great deal of simplicity and interchangeability for use in future projects.

The success of our project depended on building a platform that had indisputable structural integrity, minimal drag and weight, allowing us to test the turbine without limitations on UNH's 30 ft. test barge. Additionally, experimental measurements of the turbine's efficiency, such as torque, rpm and power generation, had to be creatively implemented into the underwater design.

The major goal of our project was to successfully design and build a structure capable of testing our sister groups' underwater VFG Turbine despite having four fewer team members than last year's group, and a smaller budget. To achieve this goal, a number of intermediate goals were determined:

- Design and build the support structure which will hold the turbine underwater
- Design and build the top frame which will attach the tripod to the barge
- Design and build a winch system capable of hoisting the tripod/turbine into place
- Mount top frame to the barge
- Perform Tank Test of tripod assembly both with and without a mock turbine weight applied to ensure structure sits true in water

- Perform Hip-Tow test of barge both with/without tripod attached to determine approximate drag of support structure

### 3 Design of Support Structure

#### 3.1 Previous Work

Research on this technology has been conducted by UNH undergraduate students for the past several years. Out of this work came a first generation VFG turbine and a test structure mounted to UNH's 30 *ft* test barge as seen in Fig. 1. However, the VFG turbine and test structure were not actually designed for each other, but rather the structure was used to test a large vertical axis turbine.

The test structure was an impressive edifice, but was not a good design for the second generation VFG turbine we wished to test. The large structure weighed over 1700 *lb* and stood at a height of over 14 *ft*. It was made from angled steel bar which had almost no consideration for drag through the water. Also, the structure was designed for a specific turbine test and hence was not made to easily assemble/disassemble and transport. With this said, the design was successful at bringing the mechanical motion of the turbine to the surface and converting it into electrical energy. They also successfully tested their turbine by mooring their test structure under the Old General Sullivan Bridge in the Piscataqua River. Using the strong tidal currents at that location, they were able to generate enough electricity to light several light bulbs.

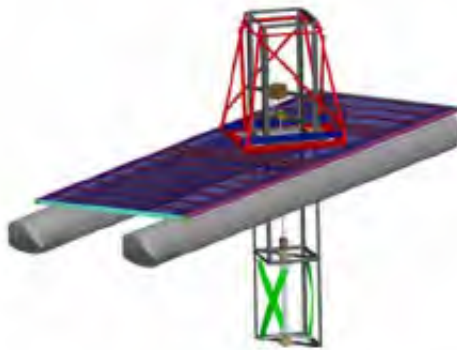


Figure 1: CAD model of old turbine testing structure mounted to UNH's barge

UNH's first generation VFG turbine was successfully built and tested last year. The group was able to build the turbine which was less than 4 *ft.* in diameter and was fitted with six NACA 0012 aluminum air foils. They were not however, able to adequately test their turbine since they were limited to test in Chase's indoor tow tank. In the tow tank, the turbine could only experience water flow at speeds just above one knot and for less than one minute at a time. Their work proved the concept and inspired this year's team to build a larger turbine that could be tested in a real ocean environment at higher water flow speeds.

The previous work of UNH's tidal energy teams encouraged the two projects of this year to continue the research into usable tidal energy. This year however, the goal was to build a structure that



Figure 2: Corrosion on old turbine test structure

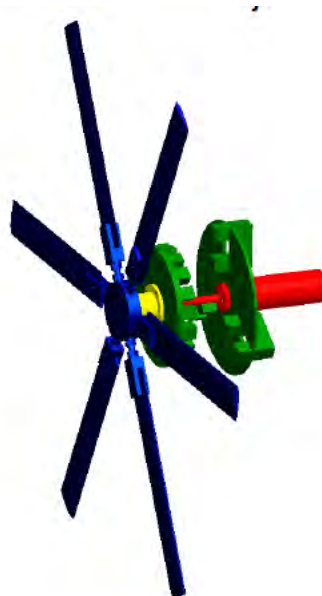


Figure 3: CAD model of UNH's first generation VFG turbine



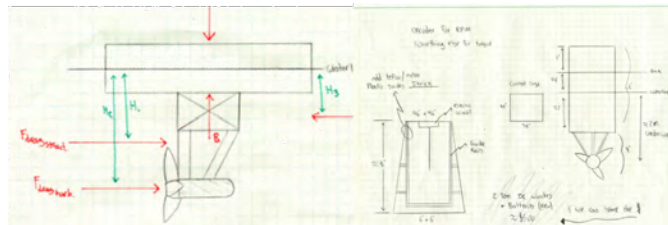
would be simple and robust, but most importantly be able to perform more credible testing on horizontal axis hydrokinetic turbines.

### 3.2 Alternate Designs

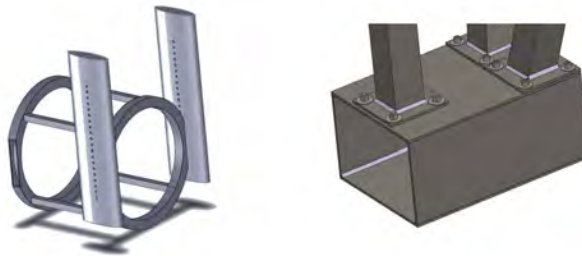
To arrive at the final design, many iterations of the design process were completed to meet the operational requirements. With each new design there were many criteria that were weighted and considered

- Ease of deployment
- Complexity in fabrication
- Overall drag
- Structural rigidity
- Cost
- Safety

Our original approach to the problem was based around utilizing last year's structure as much as possible. The initial design involved modifying the bottom half of the structure to adapt to a horizontal axis turbine as seen in Fig. 4(a). However, problems arose when the structure from last year was inspected the structure from last year and it was found to be substantially corroded and too large to move. From this point on it was decided to create a new structure from scratch that would address many of the problems from the old design such as the size/weight, drag, corrosion protection, and adaptability.



(a)



(b)

Figure 4: Several Design ideas that were never implemented

The next big step in the design process was deciding on a structure that would be stable enough to sustain a minimum of  $2400\text{ lb}_f$  at  $1.5\text{ m}$  ( $\sim 4.92\text{ ft}$ ) under the water. It was decided that a tripod design would be ideal by providing support from all directions while keeping the design simple and light. At this point the turbine group had decided to make the turbine at least  $5\text{ ft}$  feet in diameter in order to generate considerable power. This criterion led to the next big design decision. With such a large turbine, it could not be lowered through the opening on the deck of the barge and still clear the distance between the two pontoons. The chosen solution to this problem was to float part of the structure and the turbine together and lift them up from the bottom of the barge into place. With this new design, it was no longer necessary to build a massive support structure on top of the barge used to lower the frame into the water.

With the new criteria, the structure had to be as light as possible while being able to attach and detach easily from the barge. Also, the goal of the structures design was to be adaptable for use with other horizontal axis turbines, beyond the scope of this project. In order to finalize the details of the general design, a wide range of analysis was conducted.

### 3.3 Static Analysis

Before any analysis on the bolted or welded connections could be accomplished, the static forces on the deployment structure needed to be estimated. Primarily, the forces on the ends of the tripod legs needed to be solved. From prior analysis, the deployment structure is predicted to deflect a maximum of  $1/8$ " so it is justified to assume that the structure remains motionless for the analysis

The method chosen to evaluate the forces on the turbine structure followed the physical principles of statics that is

$$\Sigma F_{x,y,z} = 0 \quad \Sigma M_{x,y,z} = 0 \quad (1)$$

The deployment structure was simplified to consist of a box with three vector forces located on top, representing the force of the turbine acting through the leg's centroids. The turbine itself was mounted with bolts to the bottom of the box which was simulated by a force acting tangentially to the box's bottom face in the opposite direction of the structures motion. Also, the force of the turbine was assumed to be  $2400\text{ lb}$  which is a very conservative value and will account for a factor of safety. A coordinate grid was defined so all forces could be defined by a three dimensional vector.

It first glance, it was assumed that the front vertical leg of the structure was experiencing stress concentrations due to the tension caused by the bending of the beam. Because of this, the front beam was assumed to have a tension force directly upwards and a reaction force acting opposite of the force of the turbine. The two back support legs were assumed to have equal forces and were assumed to be in compression. Because of the legs complex angle, the reaction forces have three dimensional components. From these assumptions the forces in all three directions were added together and set equal to zero. Lastly a moment was taken about all three axis using vector cross products. The result was a matrix of equations and unknowns that could be solved. Each equation of the matrix defines the sum of the forces in a particular direction. The results can be seen in Tab. 1 where  $i, j, k$  represent the  $x, y, z$  axis directions.

Table 1: Forces acting on various positions

Force Location	Force (lb <sub>f</sub> )
$F_{turbine}$	2400
$F_{back,i}$	367.55
$F_{back,j}$	-899.78
$F_{back,k}$	160.77
$F_{front,i}$	1668
$F_{front,j}$	1800

**NOTE** Force of back right and left are equal with exception of k direction which has equal and opposite direction

### 3.4 Stress Concentration

In any structural member, the stresses within the material are of most concern around stress concentrations. These stress raisers disrupt the flow of stresses and cause the stress to increase significantly, which can cause yielding or fracture in the material. The two chief locations of concern are at either end of the airfoils. The front air foil takes much of the drag force at one end while it is bolted securely on the other end, making its analysis similar to that of a cantilever beam. The non-free end is supported by six, 1 in bolts, which were calculated to support the large moment at the connection. However, the rear airfoils are not supported by a large bolt configuration, but rather, they are welded to attaching plates. The free body diagrams of the airfoils can be seen below in both Fig. 5 and 6 with the location of most concerning stress concentration identified. At these locations, stress elements were used to determine the von Mises stress at that location.

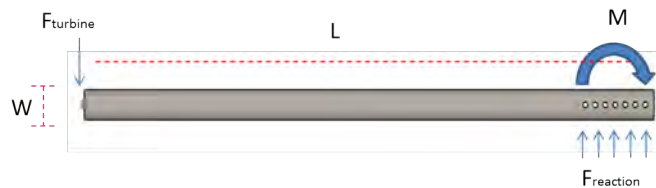


Figure 5: Free body diagram of the front airfoil

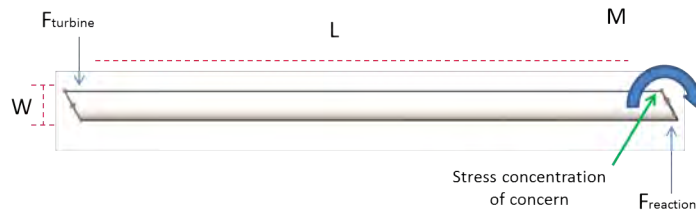


Figure 6: Free body diagram of the rear airfoils

The most critical location determined from the free body diagrams was the stress concentration located at the frame connection, (right side of the FBD), of the rear air foil. At this location the

element as seen below in Fig. 7 experiences nominal stress due to the bending moment, and shear stress due to the bending shear and direct shear.

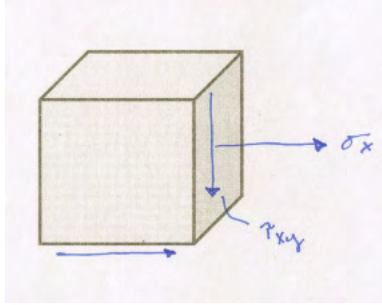


Figure 7: Stress element at stress concentration located at the end of the rear airfoil

$$\sigma_x = \sigma_{bending} = \frac{My}{I} = \frac{F_{turbine} L (\frac{W}{2})}{I} \quad (2)$$

The shear stress at this location is due to bending shear stress. At the surface the bending shear stress is ideally zero, but it was considered the maximum transverse shear stress for safety reasons. The direct shear stress is due to the reaction force at the connection which is equal to the force of the turbine.

$$\tau_{xy} = \frac{3V}{2A} + \frac{V}{A} = \frac{3 F_{turbine}}{2A} + \frac{F_{turbine}}{A} \quad (3)$$

The maximum shear stress must be found in order to solve for the principle stresses and eventually the von misses stresses.

$$\tau_{max} = \sqrt{\left(\frac{\sigma_x}{2}\right)^2 + \tau_{xy}^2} \quad (4a)$$

$$\sigma_1 = \frac{\sigma_x}{2} + \tau_{max} \quad (4b)$$

$$\sigma_2 = 0 \quad (4c)$$

$$\sigma_3 = \frac{\sigma_x}{2} - \tau_{max} \quad (4d)$$

Defining the von Misses stress to determine the actual stress value on the element.

$$\sigma_{actual} = \sigma_{von\ misses} = \sqrt{\sigma_1^2 - \sigma_1\sigma_3 + \sigma_3^2} \quad (5)$$

The actual stress at this location would be affected by the stress concentration factor of the notch. The stress concentration factor was chosen to be equal to 2.5 based on information from textbooks. The stress concentration factor is characterized by the ratio of the width of the airfoil to the width of the connecting plate, as well as the ratio of the welded fillet's radius to the width of the airfoil.

$$K_{bending} = 2.5 \quad (6)$$

The actual stress was determined by applying the stress concentration factor

$$\sigma_{actual} = (\sigma_{nominal} + \sigma_{bending})K_{bending} \quad (7)$$

## 4 SolidWorks FEA Analysis

Within SolidWorks, CAD model construction/modification, fluid flow analysis, FEA analysis, and optimization design studies were utilized to perform more detailed analysis of the structure. The conclusions derived from SolidWorks were also be validated with analytical calculations using the fundamental principles of mechanics.

A basic model of the tripod design had been conceived and modeled using square tubing as the tripod legs. Knowing that the tripod legs are key components affecting the structure's mechanics, two additional feasible designs were studied in order to determine the best fit for this application. The studies determined the best beam design based on each beam's fluid drag, maximum deflection, and weight.

### 4.1 Flow Simulations

SolidWorks Flow Simulation software was utilized to help determine a support strut design that minimized fluid drag. Three design scenarios were tested including square bar tubing, triangular faced tubing and an ellipse airfoil. Particular attention was paid to the pressure drag, which occurs at the front of the strut, and the separation area which occurs directly behind the strut. When deployed, this support structure will need to support up to 2,400  $lb_f$  at its base, so it is critical that the distributed force from drag be as small as possible. Each simulation was run with water as the fluid moving past the geometric shape at a speed of 6 *knots*. The geometric shapes tested have the following dimensions:

Table 2: Table of Dimensions for each Geometric Shape

	<i>Width/Chord</i> (in)	<i>Length</i> (in)
<i>Square</i>	3.0	3.0
<i>Triangle + Square</i>	3.0	6.0
<i>Ellipse Airfoil</i>	1.50	6.0

Each SolidWorks Flow Simulation uses the following Flow Simulation Assumptions:

- External Flow (Exclude Cavities w/o Flow Conditions)
- Adiabatic Wall Boundary Condition
- Water was chosen as Fluid Medium
- 0  $\mu m$  Surface Roughness

- 6 *knots* Flow Speed in X-Direction

To ensure that the results obtained from the SolidWorks analysis were correct, hand calculations were performed to calculate the total force of drag on the beam. The force due to drag can be calculated using the following equation,

$$F_{drag} = \frac{1}{2}\rho V^2 C_d A_{face} \quad (8)$$

where  $\rho$  is the density of salt water,  $V$  is the speed of the fluid (in this case equal to the maximum speed the turbine will be subjected to of 6 *knots*),  $C_d$  is the coefficient of drag which varies for each geometric shape and  $A_{face}$  is the face area subjected to the flow.

From both the Hand Calculations and the SolidWorks Flow Analysis, the geometric shape with the best properties for our application is the Ellipse Airfoil. This can better be described by Table 3 below.

Table 3: Table of Calculated Drag vs. SolidWorks Analysis

	<i>SolidWorks</i> ( $F_d$ ) ( $lb_f$ )	<i>Hand Calculations</i> ( $F_d$ ) ( $lb_f$ )	% <i>Difference</i>	$C_d$ ( <i>Hand Calcs</i> )
<i>Square</i>	248.55	239.68	0.0357	1.05
<i>Triangle + Square</i>	97.61	102.72	0.0498	0.45
<i>Ellipse Airfoil</i>	15.73	14.84	0.0572	0.13

The drag on the Ellipse Airfoil ended up being 5X less than the drag on the square bar with the triangle, and 12X less than that of just the square bar. As the drag on an entire Ellipse Airfoil strut is roughly 15.75 *lb*, it is negligible compared to the total force the turbine puts on the structure of 2,400 *lb<sub>f</sub>*. Lastly, Hand Calculations were all within 5% of the SolidWorks results, indicating an accurate analysis.

## Square Bar Tubing

Square Bar Tubing was first selected as the preferred strut material because it was cheap and strong. However, it was obvious that square bar tubing would also have significant drag. In order to make sure that the drag force was not too excessive, a SolidWorks Flow Analysis was performed as seen below in Fig. 8.

The square bar tubing experiences both a significant high-pressure buildup and a large separation area, as shown in Figures 8(a) and 8(b) respectfully. It is clear from this figure that square bar tubing is not the best geometric shape to use.

## Triangular Faced Tubing

It was clear that the Square Bar Tubing had too much drag to be useable. In order to alleviate some of that drag, a triangle was added on the front of the tube to try and reduce the pressure drag on the front of the beam.

Notice how the pressure drag has decreased in area significantly over the Square Bar Tubing as seen in Fig. 9(a). However, due the the flat back, there is still a large separation area seen in

Fig. 9(b) Overall, adding the triangle to the front of the square tubing cut down pressure drag significantly, but did not address the separation area. In order to alleviate both the pressure drag and separation area, the back of the square needed to be modified as well.

### Ellipse Airfoil

While the Triangle did decrease the pressure drag on the front of the strut, it did not alleviate the separation area which occurred on the back side of the strut. To try and decrease this area as much as possible, a geometric ellipse was used. This should decrease the separation point significantly.

From Fig. 10, it's clear that the Ellipse Airfoil is the best overall shape to use. It completely rid the strut of separation area, and while there is still some pressure drag on the front of the strut, it is insignificant compared to the force of drag the turbine puts on the structure. It was unknown whether the benefits of an airfoil would outweigh the cost. Obviously, an airfoil is going to have much less drag than the other shapes, but there was concern that manufacturing costs would be too high. Clearly from these results, airfoils are worth the extra money.

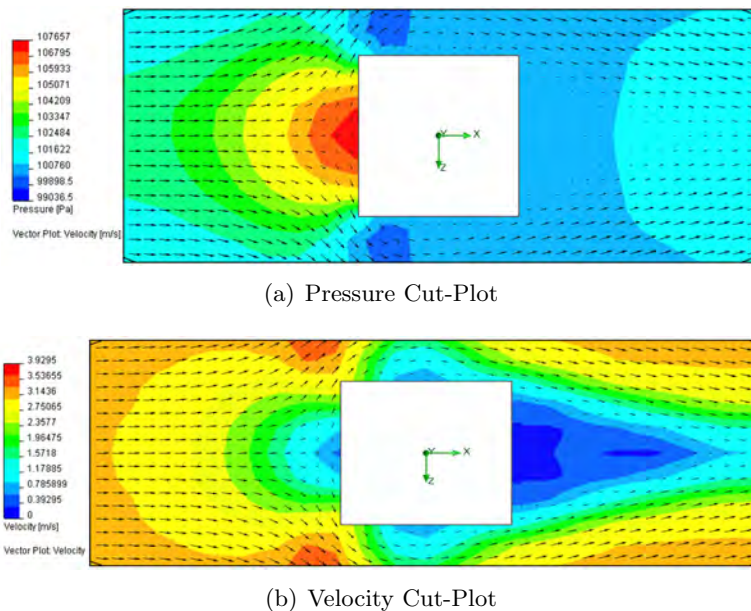
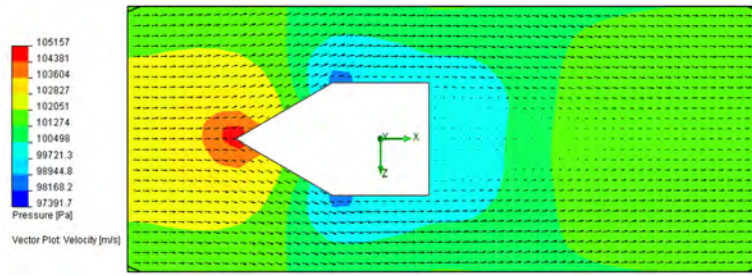
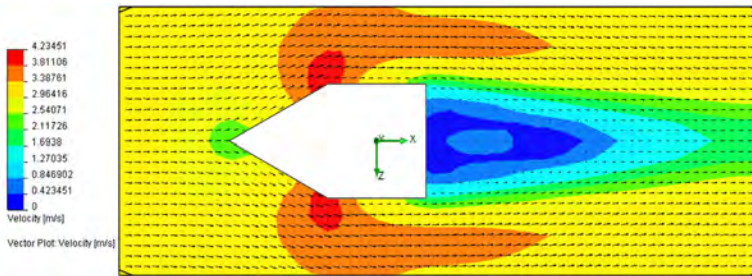


Figure 8: Pressure and Velocity cut plots for Flow Analysis over Square Bar Tubing

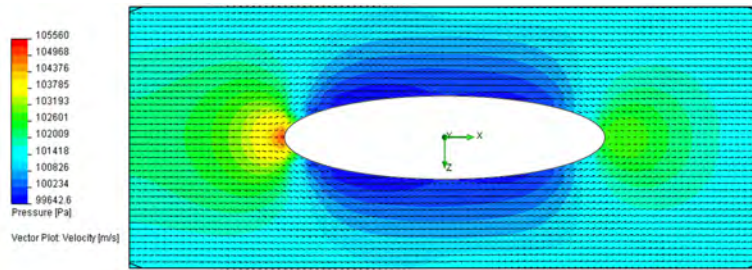


(a) Pressure Cut-Plot

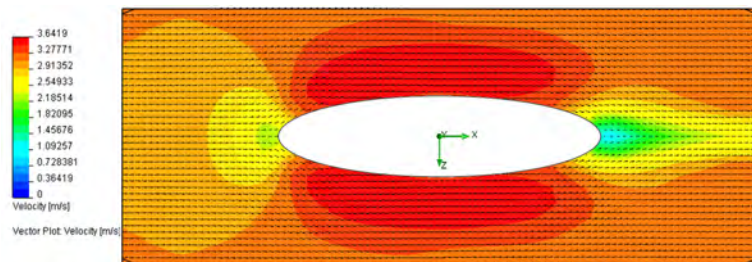


(b) Velocity Cut-Plot

Figure 9: Pressure and Velocity cut plots for Flow Analysis over Triangular Faced Tubing



(a) Pressure Cut-Plot



(b) Velocity Cut-Plot

Figure 10: Pressure and Velocity cut plots for Flow Analysis over Ellipse Airfoil



## 4.2 Displacement Analysis

When the deployment structure is operational, a key criteria that must be met is to minimize deflection so the axis of the turbine remains horizontal. When determining an ideal deployment structure, the tripod legs (struts) are the significant design components that will affect the deflection of the entire structure. The overall deflection of the structure was examined through a SolidWorks simulation of the entire structure.

The three tripod leg designs that were chosen to be analyzed were a simple square beam, a triangular faced beam, and an ellipse airfoil, which can be seen in Fig. 11 below and are similar to the models used in the flow simulations.

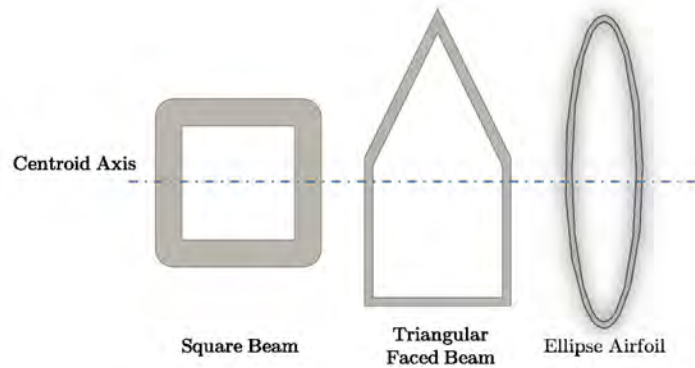


Figure 11: Cross Section of Beam Designs

When determining the deflection of a cantilever beam, the beams second moment of area is the key parameter. The second moment of area,  $I_\lambda$ , is dependent on the beams cross sectional area and can be found for any cross section using the equation,

$$I_\lambda = \int n^2 dA, \quad (9)$$

where  $dA$  is the elemental area and  $n$  is the perpendicular distance from the axis  $\lambda$  to the element  $dA$ . For this scenario the second moment of area is taken about the centroid axis as seen above in Fig. 11. To find the second moment of area of the beam cross sections, the composite of simple shapes can be used with the parallel axis theorem. The parallel axis theorem is useful when the centroid axis is not symmetrically in the center of the objects cross section like as in the triangular faced beam. The mathematical expression for the parallel axis theorem, solving for the area moment of inertia about any parallel axis  $I_z$  is given by

$$I_z = I_x + Ar^2, \quad (10)$$

where  $I_x$  is the area moment of inertia relative to the objects centroid,  $A$  is the area of the plane region, and  $r$  is the distance from the  $z$  axis to the centroid  $x$  axis. An image of the simulation setup on the triangular faced beam can be seen in Fig. 12 below.

The design study updated the dimensions of all three models and the results of all three studies. The maximum displacement of each of the beams needed to be verified analytically before the chosen

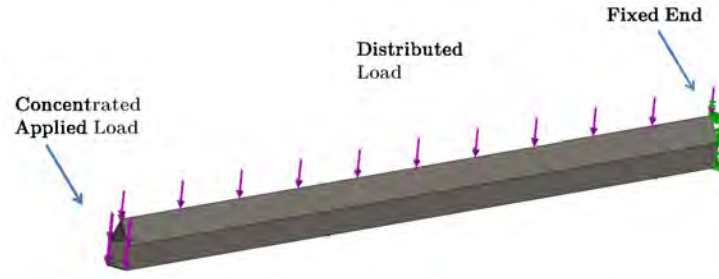


Figure 12: SolidWorks FEA Setup of Triangular Faced Beam

beam design could be fully justified. For the cantilever beam model, the maximum deflection  $\delta_{max}$  of a beam fixed at one end for both a point load at the free end of the beam and a distributed load along the length of the beam can be determined using the following equations.

### Point Load

$$\delta_{max} = \frac{Pl^3}{3EI}, \quad (11)$$

where  $P$  is the concentrated load at free end,  $l$  is the length of the beam,  $E$  is the modulus of elasticity, and  $I$  is the second moment of area.

### Distributed load

$$\delta_{max} = \frac{\omega l^4}{8EI}, \quad (12)$$

where  $\omega$  is the distributed load. When analyzing a beam with both a concentrated load and a distributed load, the superposition method can be used. The superposition method states that the beam with multiple loadings has a deflection equal to the sum of the deflections due to each loading independently. For the given scenario, the total deflection is given by the equation

### Combined loading

$$\delta_{max} = \frac{l^3(8P + 3\omega l)}{24EI}, \quad (13)$$

Overall, the results from the study provided sound information used to decide on a beam design. The results from the SolidWorks simulations were also justified by the results of the analytical calculations.

It is clear that the ellipse airfoil requires the least mass to meet the deflection criteria. This is due to the ellipse airfoils large second moment of area about the centroid axis. So far, the ellipse airfoil not only has the least deflection, but also has the lowest fluid drag associated with it. Before the final beam design is chosen, the three deflection scenarios were run in SolidWorks and compared to the analytical calculations as seen in Table 4

Table 4: Table of comparison between SolidWorks and analytical deflection calculations

	<i>Simulated Deflection (in)</i>	<i>Analytical Deflection (in)</i>	<i>% Difference</i>
<b><i>Force Drag Only</i></b>			
<i>Square</i>	0.106	0.306	65.55
<i>Triangular Faced</i>	0.012	0.147	91.96
<i>Ellipse Airfoil</i>	0.008	0.019	60.0
<b><i>Applied Load Only</i></b>			
<i>Square</i>	0.995	0.959	3.69
<i>Triangular Faced</i>	1.167	1.173	0.47
<i>Ellipse Airfoil</i>	1.091	0.978	11.51
<b><i>Both Loading Conditions</i></b>			
<i>Square</i>	1.101	1.266	13.03
<i>Triangular Faced</i>	1.177	1.319	10.80
<i>Ellipse Airfoil</i>	1.098	0.998	10.10

From Table 4 it is evident that the analytical calculations are similar to the simulated results. The analytical calculations used the analytical determined second moment of area which accounts for some of the error. It also should be noted that the largest percent differences were observed when calculating the drag force deflection only. This is due to the small deflections of this scenario, but it should be noted that the differences are within several millimeters only.

### 4.3 FEA Analysis

To ensure accurate results during simulation, the various parts are put together exactly as they would be in real life. This involves the use of weld constraints, contact constraints (with friction), bolt constraints and no-penetration contact sets. Just as it would be in real life, each bolt is pre-torqued down with a force of  $1.25 \text{ lb} - \text{ft}$ . When bolts are pre-torqued, it increases the surface friction between the metal bolt plates and the steel box, releasing some of the stress on the bolts themselves. Contact constraints let SolidWorks know that the plates are not a part of the steel box. The most effective way of understanding the assembly process is by looking at Fig. 13.

FEA analysis in SolidWorks was conducted on the deployment structure assembly. The goal of the model was to find a model configuration that resulted in zero yield anywhere in the model. Though some constraints remained fixed, such as the applied force and the fixed geometry, other parameters were varied to enhance the results. Ideally the model would output results that not only meet the criteria, but that were justified by the accuracy of the model to real life conditions. Though many iterations of the model analysis were performed, Fig. 14 highlights the major progressions in the model FEA analysis.

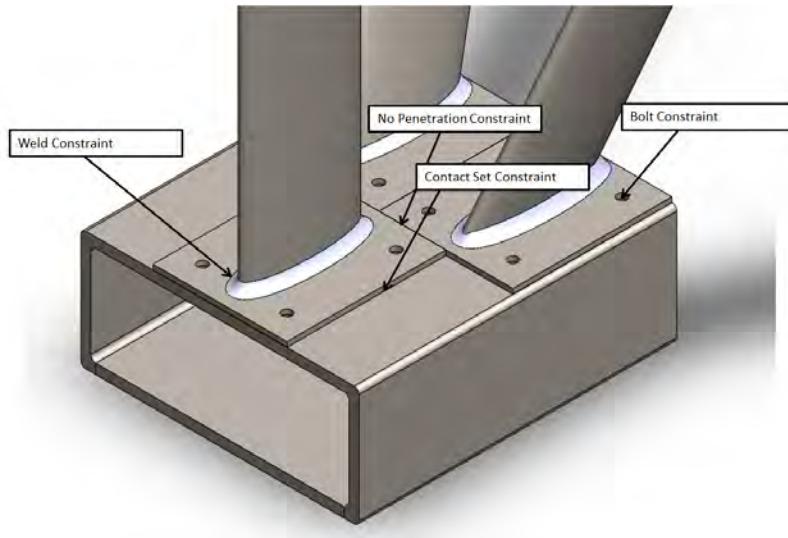


Figure 13: Figure describing setup of assembly for FEA Analysis

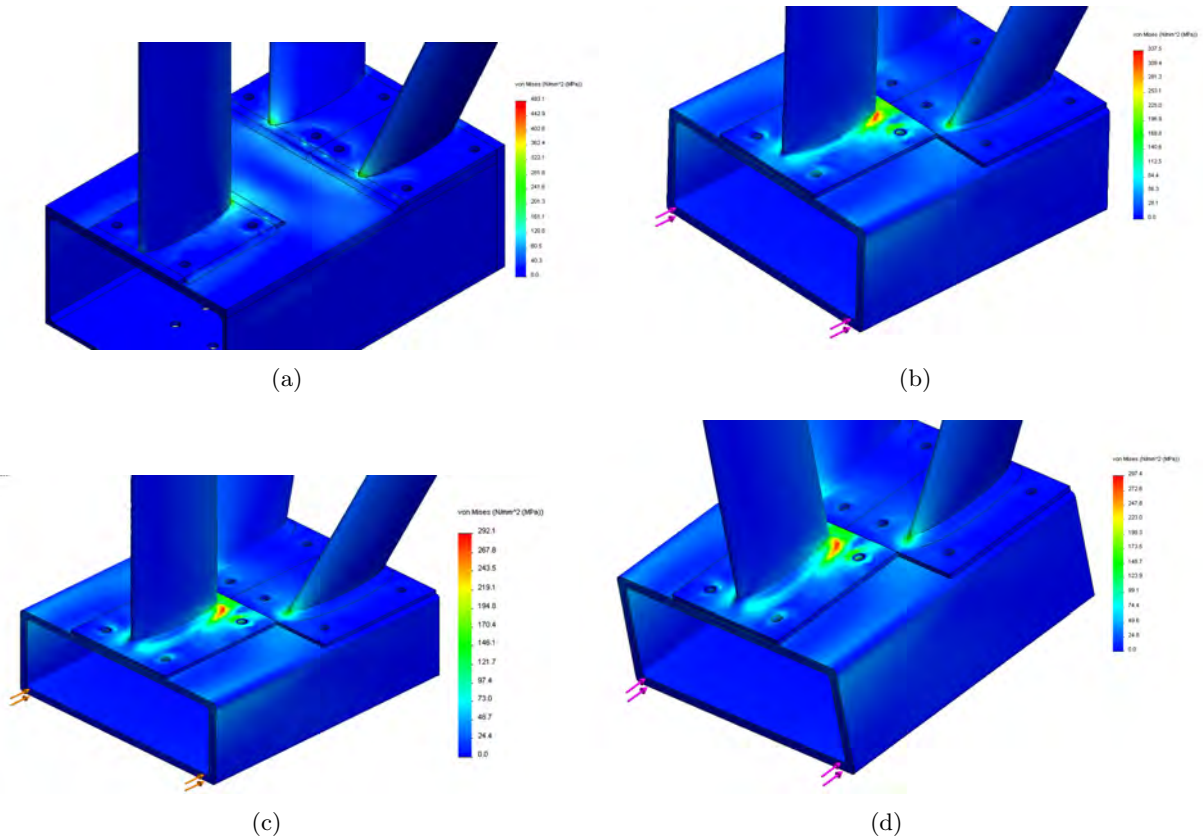


Figure 14: Progression of SolidWorks FEA Analysis Results on Assembly

- (a) The original assembly supported a 12 *in* X 8 *in* X 18 *in* steel box. This box was composed of 4 individual steel plates welded together at the corners. Simulation had no contact set constraints, bolt constraints, weld constraints and there was no specified penetration constraint preventing parts from going into one another. Welds were added to several edges along the bolt plates to try and rid the model of discontinuities. The maximum observed stress was 70.067 *ksi* focused at the ends of the ellipse airfoils.
- (b) For this model, the steel box was changed to a solid piece of steel requiring no welds. Additionally, the dimensions were modified to 14 *in* X 8 *in* X 16 *in*. These modified dimensions allowed the plates to contact each other, decreasing the stress in between the front and back struts. The ellipse airfoils were welded to the steel bolt plates using a standard 0.25 *in* fillet weld. The maximum stress concentration was located directly on the fillet weld on the back side of the front ellipse airfoil and had a magnitude of 48.950 *ksi*.
- (c) To reduce this stress concentration even further, the fillet welds were changed to a concave fillet weld so that it minimized the discontinuities of the FEA process. These welds also grew in size to 0.44 *in* in an attempt to increase the strength of that section. Additionally, to reduce the moment around the stress concentration, the height of the steel box was reduced from 8 *in* to 6 *in*. The maximum stress was still located in the same location as the previous trial, however the maximum stress concentration was reduced to 42.365 *ksi*.
- (d) In the previous 3 trials, the weld material defaulted to the same material used by the assembly (*AISI 1010 Hot Rolled Steel*). This steel is relatively soft, and is unrealistic for a weld. In this trial, the weld material was changed to *AISI 1020 Cold Rolled Steel*, which had a yield strength of 50.763 *ksi*. Although the weld was stronger, the geometry of the structure resulted in nearly identical stress concentrations as the previous trial. However, unlike the previous trials, this weld will not yield. Therefore the assembly meets the required criteria.

## 5 Connection Analysis

The entire structure is held together by either bolted or welded connections that had to be analyzed in the design to ensure the integrity of the connections. To verify the design, careful considerations and assumptions had to be taken when simplifying the analysis. All key assumptions are stated and are conservative to what is actually expected on the deployment structure.

### 5.1 Bolted Connections

The methods used to determine the bolt forces were derived from primarily the *Applied Structural Steel Design 3<sup>rd</sup> edition*. Also to determine the allowable stress on bolt configurations the *Manual of Steel Construction Allowable Stress Design 9<sup>th</sup> (ASDM) edition* was utilized.

#### Front Leg: Box Connection

From the force calculations on the deployment structure, there was a force on the bolted connection at this location that acted in both shear and in tension. Since the structure does bend, and that the applied force of the turbine acts only 6 *in* from this connection, it was assumed that the legs were fixed at the top location and that there was no moment at the bottom connections. This decision had to be made and it was clear that the moment forces were most relevant at the top connections. The forces on the bolts are a composite of shear and tension forces, but for analysis each could be considered independently.

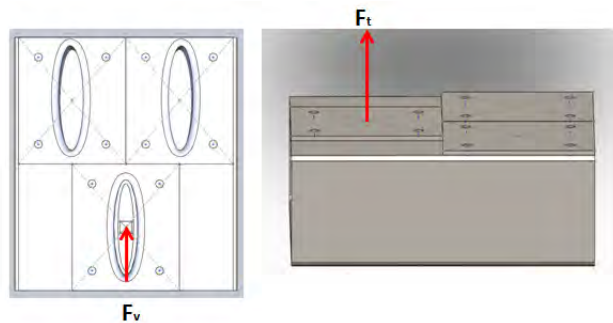


Figure 15: Free body diagram of the front airfoil connection to the mounting box

#### Back Legs: Box Connection

For the back supports, the members are assumed to be in compression which exerts a reaction force on the bolted connections in all three dimensions. For this scenario, instead of considering the bolts to be in pure tension or pure shear, the actual analysis combines the dimensional forces. The force does act at the centroid of the airfoil, which is also the centroid of the bolt group meaning there is no eccentricity in the analysis.

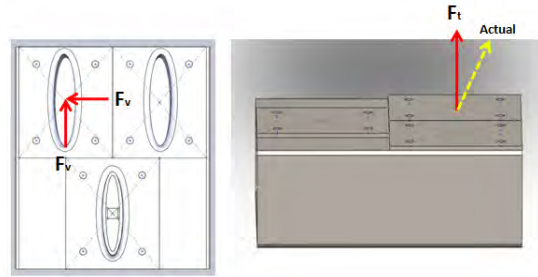


Figure 16: Free body diagram of the rear airfoil connection to the mounting box

### Back Legs: Top Connection

The top bolted connections of the back legs of the turbine structure are a bit more complicated. Since it was defined that the top of the legs are fixed while the other end is free to move, a moment is induced by the turbine and eccentricity must be considered. The connecting plate wants to separate from upper frame due to this moment. Since the member is in compression, there was no tension force to analyze directly.

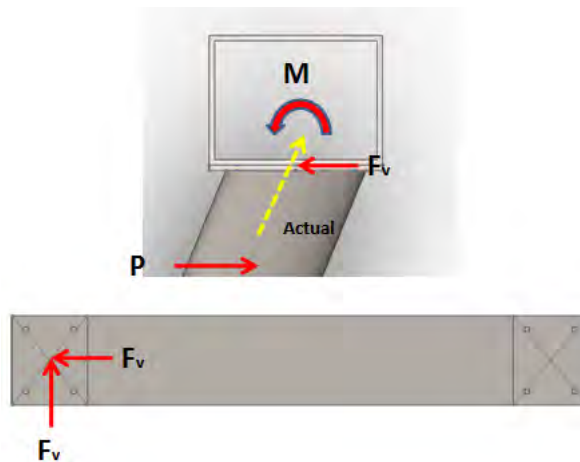


Figure 17: Free body diagram of the rear airfoil connection to the top frame

### Front Legs: Top Connection

The top bolted connection of the front support also is effected by the moment induced by the force at the bottom of the leg. Eccentricity must also be considered and the moment increases the shear force on the bolts which have no tension forces. There are also two shear planes for this scenario. Since the bolts were expected to experience large shear forces due to the moment. 1 in diameter bolts were selected in the design. This can best be seen in Fig. 18.

### Frame Bolts

This scenario combines all the scenarios dealt with since. The bolt group, (not illustrated), will hold the deployment structure to the frame mounted to the boat. This problem deals with the

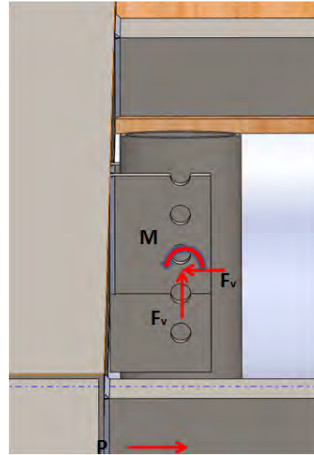


Figure 18: Free body diagram of the front airfoil connection to the top frame

compressive force of the back legs on the frame. This force acts eccentric to the bolt group in two directions inducing two moments. One moment causes the prying of the plate on the frame, while the other adds to the shear force. The bolts experience many points of both shear and tension that can be added vectorally. It is important to note that this connection does not experience the large moment forces that the previous connections withstand. Since the frame is in two pieces the moment is minor and the neutral axis becomes the plane that separates the two parts of the frame.

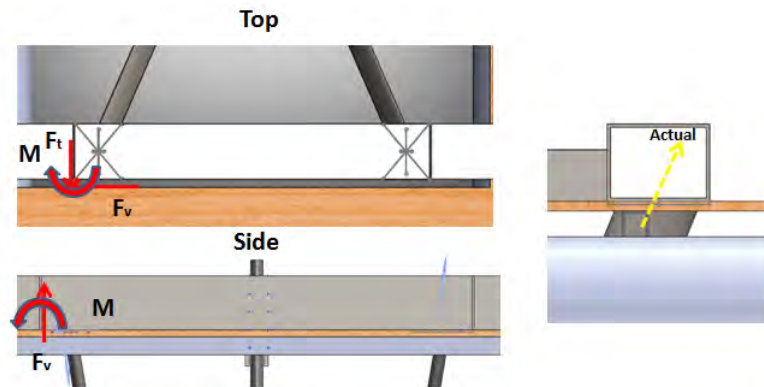


Figure 19: Free body diagram of the bolted connection holding the frame together

## 5.2 Welded Connections

The majority of the components of the support structure are welded together. As such, it's important to ensure the deployment structure will be structurally sound during testing. From previous SolidWorks simulations, there had been significant stress concentrations along the rear of the front support strut and the front of the rear support struts. These stress concentrations exceeded the yield stress of the material in some areas, and were later discovered to be caused by the area going to zero at the tips of the airfoils. Through the calculations, these stress concentrations were also proven to be mostly imaginary. Using the forces calculated during the Bolt Analysis, various welds



were analyzed against failure. These analyses provided the necessary information to design the various parts of the welds such as the leg and throat size in such a way as to successfully and safely stand up to the punishment the deployment structure will encounter during testing. Lastly, convex fillet welds were used during all calculations because they are less prone to cracking as a result of the shrinking during cooling compared with convex fillet welds. The various parts of a standard convex fillet weld can be seen below in Fig. 20.

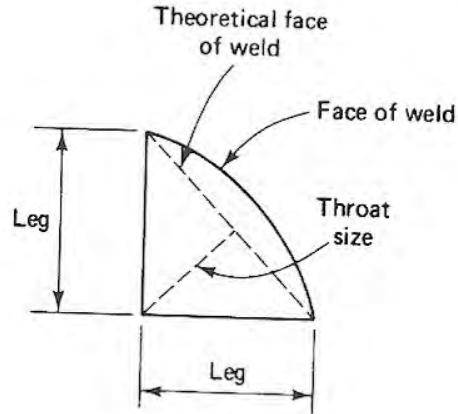


Figure 20: Various parts of a Convex Fillet Weld

In order to ensure the strongest connection possible, each part of the weld needs to be individually analyzed and calculated. Also, notice how there is both a theoretical weld face and a normal weld face. The difference between them is that the normal weld face is said to add no extra strength to the weld. Therefore, all calculations dealing with a fillet weld use only the theoretical weld face. In order to design a suitable weld for our structures, basic parts of the weld such as the Leg and Throat sizes needed to be determined. These can be calculated with Eqns. 14 and 15 below:

$$\text{Leg Size} = 2 * (\text{thickness plate}) \quad (14)$$

$$\text{Effective Throat Size} = \sin(\theta) * \text{leg size} \quad (15)$$

It is important to note that Eqn. 14 can only be used to calculate the leg size of pieces with equal thicknesses as we have in our case. Additionally, the angle  $\theta$  is the angle between the two plates and must be within the bounds of  $60^\circ \Rightarrow 120^\circ$  to be considered a fillet weld. For the case of the tripod, all angles were considered to be  $90^\circ$ . With the throat size calculated, the strength of the fillet weld per linear inch could be calculated using Eqn. 16 below:

$$P = (0.3)(F_u)(\sin(\theta))(\text{leg size}) \quad (16)$$

where  $P$  is the strength of the fillet weld per linear inch and  $F_u$  is the specified minimal tensile strength of the electrode used to weld the material. Knowing the overall length of the weld (Perimeter in our case), the overall weld capacity of the fillet weld could be calculated using Eqn. 17 below:

$$Weld\ Capacity = (P)(Length\ Weld) \quad (17)$$

With the basic design of the weld determined, case specific calculations could be performed. To keep our options open, calculations were performed for a number of different cases, including:

- Welding the Attaching Plates to the Box
- Welding the Attaching Plates to the Airfoil Struts
- Considering the moment at the Top Plates/Struts

The results of these calculations can be seen below in Tab. 5.

Table 5: End Results from Weld Calculations

<b>Item</b>	<b>Value</b>	<b>Units</b>
<i>Leg Size</i>	0.25	( <i>Inches</i> )
<i>Effective Throat Distance</i>	0.178 ( <sup>3</sup> / <sub>16</sub> ")	( <i>Inches</i> )
<i>Strength Fillet Weld per Inch (P)</i>	3.18	( <i>Kips/Inch</i> )
<i>Weld Capacity (Attach Plates)</i>	93.81	( <i>Kips</i> )
<i>Weld Capacity (Struts)</i>	39.75	( <i>Kips</i> )
<i>Total Capacity (Attach Plates)</i>	180.75	( <i>Ksi</i> )
<i>Total Capacity (Top Struts)</i>	105	( <i>Ksi</i> )
<i>Total Capacity (Top Struts + Plates)</i>	285.75	( <i>Ksi</i> )
<i>Total Capacity (Bottom Struts)</i>	93.75	( <i>Ksi</i> )
<i>Force on Weld from Moment (M)</i>	0.4733	( <i>Kips/Inch</i> )
<i>Total Force from M</i>	5.9163	( <i>Kips</i> )

As seen above in Tab. 5, it is clear that the individual welds hve a weld capacity much higher than any force they will experience. In summary, the welds will be strong enough to successfully take the loads they will experience during deployment. It is important to note that the top frame was not considered during calculations. This is because the frame does not experience the force the tripod does, and it was fabricated with particularly large welds. Also important to note is that since these calculations were performed, four gussets were added to the area surrounding the plate/airfoil connections as this is where the majority of our stress concentrations were during simulations.

## 6 Additional Analysis

### 6.1 Buoyancy Calculations

In order to maximize the maximum amount of weight the structure could support, we needed to make the tripod as light as possible in the water. To aid in this, the middle frame and front airfoil were both filled with marine grade foam. This foam is designed to help keep small boats afloat in the event of a rollover and has a buoyancy of roughly  $60 \text{ lb}_f / \text{ft}^3$ . Thus, the total buoyancy added by the foam to our structure can be found using Eqn. ?? below.

The results of the initial buoyancy calculations can be seen below in Tab. 6.

Table 6: Buoyancy Calculations of each part of Tripod

<b>Part</b>	<b>Volume (ft<sup>3</sup>)</b>	<b>B<sub>f</sub> (lb<sub>f</sub>)</b>
<i>Front Airfoil</i>	0.2974	17.8418
<i>Rear Airfoils</i>	0.3026	18.1548 ( <i>each</i> )
<i>Middle Frame</i>	0.9429	56.5755

This table includes the buoyancy calculations for each part of the tripod, including the rear airfoils. Originally, the rear airfoils as well, but this was deemed impractical as they were already air-tight. From our calculations, the approximate added buoyancy of the foam was  $74.42 \text{ lb}_f$  from the front airfoil and middle frame added together. This was partially seen during initial pool testing of the completed tripod where it weighed in at  $360 \text{ lb}$  in air and only  $220 \text{ lb}$  in water.

Knowing the buoyancy of each member was critical in determining how the structure was going to want to sit in the water. Roughly  $1/3$  of the weight of the tripod is hanging over the back meaning that there is a tendency for the object to want to rotate around its center of mass. We needed to determine how big this tendency was, especially when it was in the water. In order to calculate this, the center of mass needed to be calculated for both the entire assembly and each individual part as they provide important reference points. Additionally, both the total weight and total buoyancy (if any) were calculated of each part. Combining this information with the geometry of the structure yielded an overall moment with respect to the x-axis of  $579.13 \text{ lb} - \text{ft}$  (NOTE: This was the calculated moment including the turbine assembly, assuming a weight of  $200 \text{ lb}$ ). Though the moment may seem high, it's about equal to the weight of the two structures. Thus, as long as the buoy's we use during testing have a capacity of at least  $579 \text{ lb}$ , the tripod assembly will be able to stay level in the water. For more information on Buoyancy Calculations, please refer to the Appendix.

In order to ensure that the tripod stayed level in the air involved careful calculations of cable length. Each leg of the tripod has a stainless steel eyebolt welded onto it providing the attachment point of each cable. The individual cable lengths needed to be calculated in such a way that they would be able to counteract the moment calculated earlier. Using basic geometry of non-right triangles, the front cable length was calculated to be  $55.6''$  long and the rear cable lengths was calculated to be  $66.4''$ . Although these lengths should counteract the moment, we wanted the lengths to be able to be varied depending on the load applied. To ensure this could happen, turnbuckles were used to allow the length to change.

## 6.2 Measuring Rotational Speed of the Rotor

In order to test the efficiency of the second generation VFG turbine, the Torque vs. RPM needed to be measured in real time. The chosen device to measure the RPM of the turbine was a laser sensor that detects reflective tape as it passes by the sensor. A series of experiments were conducted to determine if a rotational speed measuring device was capable of being implemented on the VFG turbine. As this type of turbine has a rotor that is variably displaced axially with respect to a fixed stator, traditional measuring devices were not applicable.

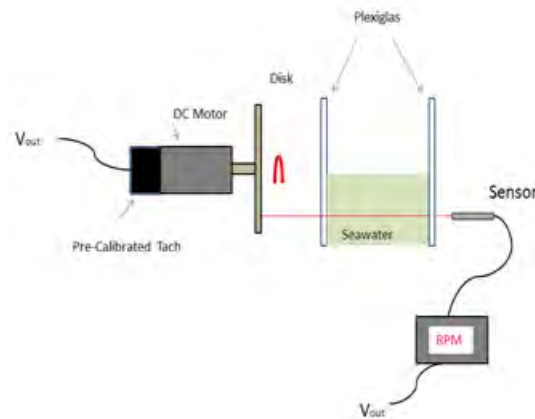


Figure 21: Diagram of the front laser tachometer device test setup

Overall, the laser optical rotational measuring device proved to be sufficiently accurate for its intended application. In order to properly compare the laser-tachometers output to that of the motor-tachometer, the motor-tachometer first had to be calibrated. From this calibration, the sensitivity of the motor-tachometer was found to be  $0.00302 \text{ volts}/RPM$ . The laser-tachometer was then calibrated and found to have a sensitivity of  $.00967 \text{ volts}/RPM$  which was slightly lower than the manufactures indicated sensitivity of  $0.01 \text{ volts}/RPM$ .

When testing the accuracy of the device at varying distances, it was found that the device is inaccurate for distances less than  $3 \text{ in}$  and is accurate to at least  $48 \text{ in}$ . The percent differences of the laser-tachometers measured rotational speed compared to that of the motor-tachometers is seen below in Tab. 7.

Table 7: Comparing Laser Tachometer to Motor Tachometer

<b>X (in)</b>	<b>% Difference</b>	<b>X (in)</b>	<b>% Difference</b>	<b>X (in)</b>	<b>% Difference</b>
0.5	63.016	3.0	0.323	12.0	0.784
1.0	27.038	4.0	0.714	24.0	0.739
1.5	29.310	5.0	0.451	36.0	0.858
2.0	0.418	6.0	0.431	48.0	0.827

A rotational speed transient of both decreasing (set 1) and increasing (set 2) speeds were measured by both tachometers. The measured responses from the laser-tachometer were then compared to that of the motor-tachometer. The measured time constants from the laser-tachometer were all within 10% of those measured from the motor-tachometer as seen below in Tab. 8. This percentage equates to less than  $0.01 \text{ sec}$  which for the intended application can be considered negligible.

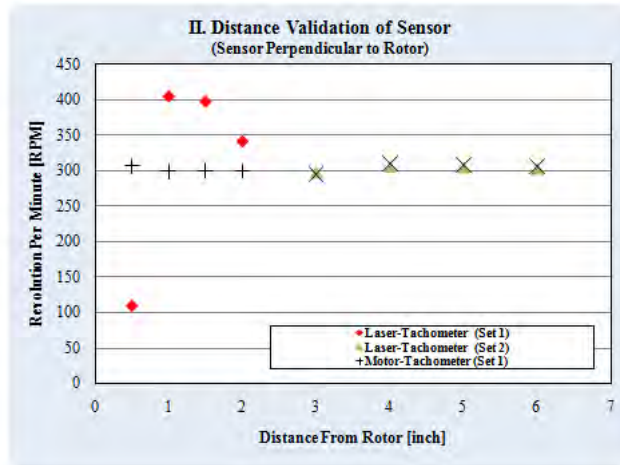


Figure 22: Plot comparing the accuracy of the laser tachometer at various distances

Table 8: Measuring Respective Transient Accuracy

Set	Trial	Transient Type	Time Constant		% Difference
			$(\tau)_m$	$(\tau)_L$	
1	1	<i>Decreasing</i>	0.878	0.933	6.264
	2	<i>Decreasing</i>	0.886	0.9627	8.657
	3	<i>Decreasing</i>	0.931	0.986	5.908
<b>Average</b>			<b>0.898</b>	<b>0.961</b>	<b>6.479</b>
1	1	<i>Increasing</i>	0.7314	0.8008	9.489
	2	<i>Increasing</i>	0.797	0.867	8.783
	3	<i>Increasing</i>	0.6881	0.7379	7.237
<b>Average</b>			<b>0.739</b>	<b>0.802</b>	<b>7.865</b>

NOTE: Subscripts  $L$  and  $m$  represent values measured by the laser and motor respectively

Lastly, to emulate the underwater environment, the device was tested through several mediums and at various angles with respect to the rotating cardboard rotor. The results from these trials are displayed in the following three charts below. The optical laser sensor proved accurate through both the Lexan and saltwater mediums, and therefore was validated to be implemented successfully on the VFG Turbine.

A great number of designs were compared in the beginning stages of the project. In the end a tripod structure was decided as the best solution. For the tripods legs, airfoils were used for obvious drag reasons. The box on the bottom which holds all three struts together was designed to be easy to mount to. It has a series of six holes on the bottom spaced evenly apart such that any future work with our structure can be quickly and easily adapted to fit our structure. We tried to design a structure that could be used for future projects as well, and as such we over designed it to handle a drag force of 2,400  $lb_f$ . This is far more than it will ever see during the testing of the turbine, and is equivalent to pushing a 5' diameter disk through the water at 6 knots, 10' below the surface of the water.

Table 9: Laser Angle of Attack  $0^\circ$ 

<i>Angle of Attack = 0 deg</i>			
<b>Medium</b>	<b>(RPM)<sub>L</sub></b>	<b>(RPM)<sub>m</sub></b>	<b>% Difference</b>
<i>Air</i>	290.41	288.29	0.737
<i>Lexan</i>	278.94	277.02	0.691
<i>Lexan + Water</i>	287.82	285.64	0.767

Table 10: Laser Angle of Attack  $15^\circ$ 

<i>Angle of Attack = 15 deg</i>			
<b>Medium</b>	<b>(RPM)<sub>L</sub></b>	<b>(RPM)<sub>m</sub></b>	<b>% Difference</b>
<i>Air</i>	290.31	287.96	0.817
<i>Lexan</i>	290.52	288.29	0.773
<i>Lexan + Water</i>	299.82	297.90	0.646

Table 11: Laser Angle of Attack  $45^\circ$ 

<i>Angle of Attack = 45 deg</i>			
<b>Medium</b>	<b>(RPM)<sub>L</sub></b>	<b>(RPM)<sub>m</sub></b>	<b>% Difference</b>
<i>Air</i>	284.31	281.99	0.823
<i>Lexan</i>	294.55	292.27	0.781
<i>Lexan + Water</i>	293.62	291.27	0.806

## 7 Final Design

### 7.1 Testing Site

The testing site of the underwater turbine ideally should consist of calm water with mild tidal currents. Unfortunately, our testing location is limited by the ability to transport the barge and the support structure. Thus, the testing location of the turbine was chosen to be in front of the UNH Pier which can experience currents upwards of 4 knots. The UNH Pier is located at Fort Point, in New Castle NH, directly across from the US Coast Guard Station. Completed in the summer of 2009, the new pier includes a 3-ton crane which will be used to deploy the structure for testing.

### 7.2 Assembly

The final design of the support structure allows it to be transported and assembled easily. Realizing that our structure would be in contact with salt water, all members are connected using 316 Stainless Steel Bolts. This is a major upgrade from the last group, who used high strength steel bolts (all of which rusted together). All of the members themselves are coated in both Rustoleum Rust Protecting primer and paint. Ideally, we would have liked to powder coat everything, but due to time and financial constraints, this was deemed impractical.

The tripod structure itself is designed to be assembled with just two people, starting with the box and working out to the airfoils, and finally the middle frame. The right and left rear airfoils and the box are stamped “L” and “R” to tell the user which way they attach together. The completed tripod assembly can be seen below in Fig. 23

### 7.3 Deployment Plan

The finished design of the support structure is meant to overcome the shortcomings of the barge, to allow for bigger turbines to be tested. This is due to the opening on the deck only being 60” x 69” wide. However, when the pontoons are taken into account, the opening becomes smaller to a final usable area of 60” x 64”. Thus, this opening can only have turbines of less than 5 *feet* in diameter fit through the opening. To allow larger turbines to be tested, we decided to go with a creative approach. Rather than dropping the turbines through the opening on the deck (which isn’t possible with larger turbines), the tripod structure which holds the turbines is designed to float in the water using a combination of foam filled members, and buoys. The barge then simply drives over the structure, and the structure is lifted/bolted into place using a capsum winch mounted on the deck. The tripod structure is bolted to the top frame structure, which is permanently mounted on the deck of the barge using a series of stainless steel U-Bolts.

When the structure is fully secured, the barge is then connected to the Galen J, a twenty foot small hard chine working boat owned by the University of New Hampshire for their marine programs. We will be using a technique known as a hip tow, which is when the boat is connected to the barge on the side. This method of towing the barge was chosen as it allowed the least interference on the turbine from the boats engine. This can best be seen below in Fig. 24.

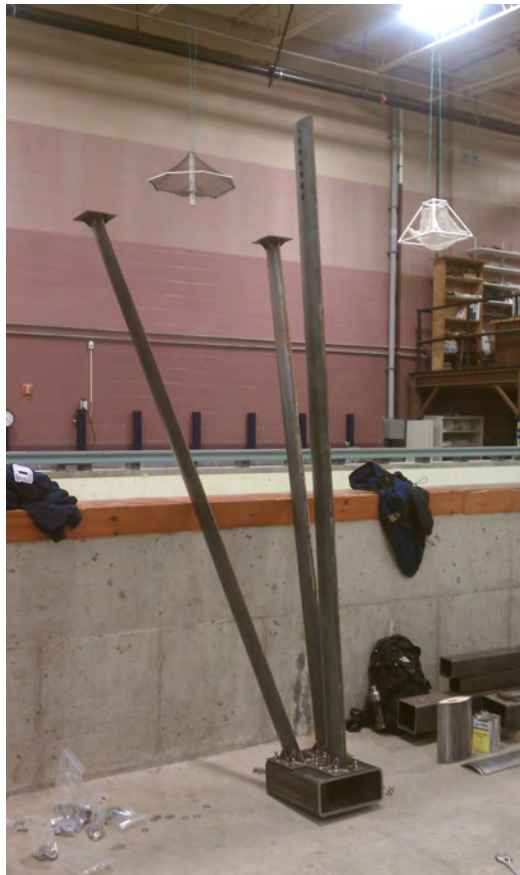


Figure 23: Completed Tripod Assembly



Figure 24: Hip-Towing the barge using the Galen J



Originally, the plan was to have the barge move on its own power by connecting an engine to the deck. However, a series of events led to this new plan. First, the bracket needed to mount an engine to the deck of the barge could not be located (Though it was later found at the UNH Pier). Next, the engine that we were going to use (a 25hp outboard borrowed from Matt Rowell) was discovered to need a lot of engine work. Lastly, additional mechanical bits would need to be added to the deck of the barge including a steering system, gas tank, and various cables/wires to make the engine run. It was decided that based on the amount of time and money it would take to make the barge usable was too much.

## 8 Construction of Support Structure

### 8.1 Airfoils

Airfoils were chosen as the support struts to significantly cut down on drag from last years angle iron structure. They are fabricated using two pieces of  $\frac{1}{8}$ " thick sheet steel approximately 106" in length. Each piece of steel is then incrementally bent using a hydraulic brake until they reach the shape of a half airfoil. Lastly, two sections are welded together along the edges using a MIG Welder. Fig. 25 below shows the three completed airfoil struts along with two extra airfoil half-sections.



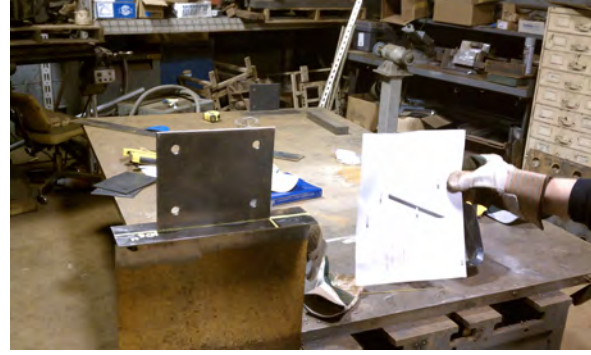
Figure 25: The three completed airfoil struts and two extra sections

Before the plates used to connect the airfoils to the rest of the structure could be added, the rear airfoils required two compound angles and the front airfoil required seven 1" holes at the top to connect to the top frame. The first mitered angles and the seven holes were cut using a water jet machine. A water jet machine uses a mixture of special abrasive powder and pressurized water ( $\sim 90,000$  psi) to cut material up to 12" thick. After the initial angles were cut, the second angles were added using a mitered band saw. With the compound angles successfully added, the plates could be added. To ensure that the airfoils matched up to the digital design, a jig was created. The water jet machine and our jig can be seen below in Fig: 26 below.

With the airfoil struts welded together, the next step was to weld the plates on the bottom of



(a) Water Jet Machine



(b) Assembly JIG

Figure 26: Water Jet machine and JIG for assembling airfoils

each side. These plates were  $\frac{1}{4}$ " thick pieces of steel, and are used to attach the airfoils to the rest of the structure using  $\frac{1}{2}$ " stainless steel bolts. Additional gussets were added to this critical connection to ensure the airfoils would have sufficient strength to withstand testing. This can best be seen by Fig. 27 below. Next, stainless steel closed eyebolts were welded into the three airfoils. These eyebolts are the connection points for the lifting apparatus which consists of galvanized  $\frac{3}{16}$ " steel cable. Lastly, both the front airfoil and middle frame were filled with foam to increase the buoyancy of the structure when it's in the water. Between the two, the foam adds roughly  $75\text{ lb}_f$ , which helps bring the total weight of the tripod down from  $360\text{ lb}_f$  to a more manageable  $220\text{ lb}_f$ . (The two rear airfoils are air-tight which also adds a few pounds of buoyancy force.)



Figure 27: Plate and Gussets attached to the airfoil

## 8.2 Top Frame

The top frame is the most crucial part of the entire structure. It's designed to transmit the horizontal drag forces from the tripod/turbine assembly to the deck of the barge. These drag forces were intentionally overestimated to ensure the structure would be strong enough for future work.

It was designed to handle a  $24,000 \text{ lb} - \text{ft}$  moment ( $2,400 \text{ lb}_f \times 10'$ ). It is connected to the barge using stainless steel U-bolts. As an extra precaution, wooden  $2 \times 4$ 's were screwed against the frame to ensure the frame couldn't move laterally along the deck of the barge.

The frame consists of six pieces of  $\frac{1}{4}$ " steel rectangular tubing and two  $\frac{1}{2}$ " steel plates. Of the six pieces of frame, one is permanently connected to the tripod assembly and is how the two rear airfoils connect to the frame. This is accomplished using four  $\frac{1}{4}$ " plates and threaded rod which fit over the holes in the two frame sections. The two steel plates have seven 1" holes in them, and is how the front airfoil connects to the frame. The completed frame assembly can be seen below in Fig. 28.



Figure 28: Completed top frame assembly mounted on the barge

The frame also has two L-Brackets welded to it which can be seen in Fig. 28 (the middle frame on the tripod structure also has these). These L-Brackets help hold the middle frame to the top frame while the threaded rod's are inserted into the frames, tying them together.

### 8.3 Box

The steel box located at the bottom of the tripod is the most crucial part of the tripod assembly. It is where the three airfoils attach to as well as the object being tested. As it will need to be able to transmit a substantial load to the top frame, we designed it to be extra strong and is a  $14'' \times 6'' \times \frac{1}{2}''$  steel rectangular tube. A lot of time was spent thinking about the eight  $\frac{9}{16}''$  holes on the bottom of the box as this is where projects will attach to. We wanted to make a pattern that would be easy to adapt to, but at the same time allowing weight to be kept as close to the center of mass as possible. Weight balance is important because it will be floating in the water and we need it to sit level. The completed box can be seen below in Fig. 29.

### 8.4 Mounting on Barge

The support structure was designed to be quickly assembled/disassembled, with a minimal amount of parts being mounted to the barge. The design was based off of careful measurements taken from



Figure 29: Completed box assembly

the barge and used to design a top frame that would disperse the force on the structure to the deck of the boat. Before the frame could be securely mounted, the barges top surface needed to be stripped of last years project.

The original plan for disassembling last years project from the barge was to leave as much of the components intact as possible. This strategy proved impossible since the corrosion that had built up on all of the connections left no option but to cut away at the structure with a reciprocating saw. Evidence of disassembly difficulties can be seen in last years report, as they warned that their use of corrosive metals would make disassembly extremely difficult. The only component that was left in place on the barge was the wooden A-frame, used by hoist the tripod from the water into position.

The top frame of the structure was mounted securely to the deck of the barge using seven U-bolts, which wrapped around the sides of the frame and bolted into the wooden deck. The completed Top Frame assembly can best be seen in Fig. 28 above. The barge deck is made of aluminum square bar pieces laid horizontally in 16 *in* increments with plywood laid over the top. Because the plywood alone would not be strong enough to keep the frame in place, the U-bolts were positioned to wrap around the aluminum supports. Of the rectangular frame, three of the sides rested on the deck of the barge, with the last side hanging over the barge deck opening. This setup allowed the rotational torque felt by the top frame to be transmitted to the deck of the barge over a large surface area. The U-bolts were simply in place to keep the frame in position due to the shearing force experienced by the horizontal force of the turbine.

## 8.5 Cable/Flotation Setup

The chosen design required the bottom half of the structure to float in the water with the 150 *lb* turbine attached to the bottom. Though some buoyancy was gained by our foam filled components,

additional floatation using buoys would be needed. In order to effectively float the large structure, a design that was reliable and that could keep the structure level was needed.

The chosen design for the flotation system used cables connected to each leg of the structure creating a tripod of cables. The cables were connected to the tripod legs using carabineers that clipped into eye-bolts welded into the legs. Each cable setup consisted of two cable ends with a turn buckle center that would allow the tripod to be adjusted as needed. The cables all hooked onto a seamless stainless steel ring independently with carabineers. From the seamless ring, three 23 *in* diameter buoys were connected, which had enough buoyancy force to keep the structure afloat. The selected design had a built in factor of safety because each cable could hold the weight of the structure, and if any of the cables failed, the structure would still be supported by all the intended buoyancy force. Using steel cables can also pose safety issues during the testing phase so by using carabineers for all of our connections, the cables could be quickly unhooked if an emergency arose.

In order to determine the exact buoyancy required, the structure was connected to a 5,000 *lb* force transducer and lowered into the testing pool at Chase hall. From the testing the in-water weight of the structure was determined to be 209 *lb*. Additionally, the weight of the 150 *lb* turbine was considered and later tested using lead bricks as additional weight. Before the structure could be put into the ocean, it was essential that the structure floated perfectly level as predicted. The exact cable lengths were chosen in the design process to counter the large moment about the center of mass of the structure. When we tested the structure in the pool however, the structure experienced varying moment forces as it was lowered into the water. After adjusting cable lengths using the turn buckles, the structure was stabilized so it would stay level in the water through the entire duration of water entry.

## 8.6 Torque Measurement/Construction

In order to measure the overall efficiency of the turbine, the rotor efficiency needs to be measured during testing. This efficiency is best determined by plotting torque vs. RPM at various speeds and eventually determining the stall torque. Due to the compact design of the turbine, the linear motion of the turbine, and the difficulty with measuring underwater, the design of the final torque measuring device was devised with the help of both groups and our advisors. The construction and application of the mechanism was primarily made by the turbine group, but our role was essential during design. The final design of the torque measuring device was based off the design of a simple prone brake attached to a force transducer by a moment arm as seen below.

For the turbine, we chose to use a bicycle disk brake mounted to a free moving moment arm. This moment arm and brake have the potential to rotate, but do not since the brake is connected to a vertical steel cable/ force transducer. A brake disk was mounted to the rotating rotor of the turbine to rotate in sync with the turbine blades. As the disk brake clamps the brake disk, a force is exerted on the force transducer that can be measured and compared directly to the RPM at that instant measured by the optical laser sensor.

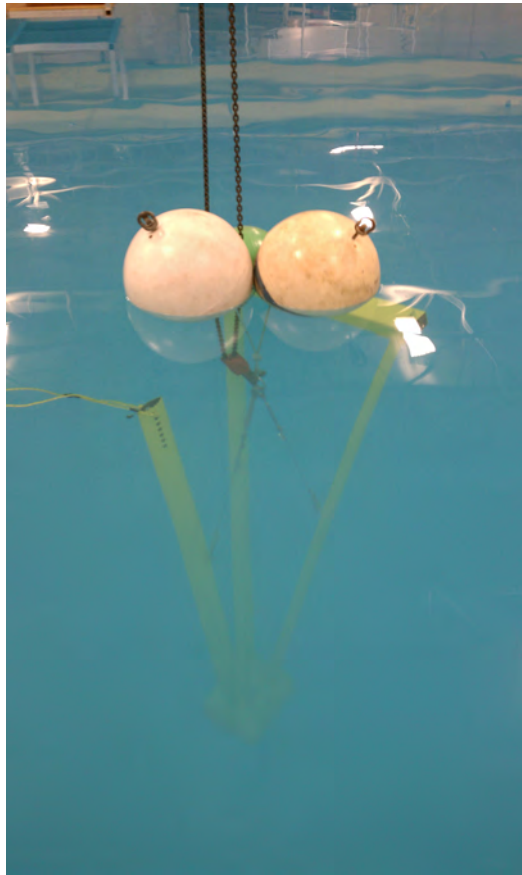
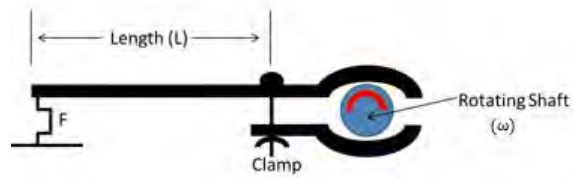


Figure 30: Flotation test of structure with simulated turbine weight



$$\text{Torque (T)} = F \times L = F \cdot L \text{ (since } 90^\circ\text{)}$$

$$\text{Power (P)} = T \cdot \omega$$

Figure 31: Simple diagram of torque transducer to be applied to turbine

## 9 Testing/Deployment

### 9.1 Drag Testing

In order to provide a more convenient package for future users of the structure, the overall drag of the structure at various speeds needed to be calculated. This was accomplished using a technique known as hip towing. This is when the pull boat (Galen J. in this case) was located on the side of the barge. A force transducer with a 5,000 *lb.* capacity was attached to a main line from the barge to the boat. This can best be seen by Fig. 32 below.



Figure 32: Hip Tow setup with Galen J. boat and Force Transducer

Two trials were performed. The first trial did not have the tripod structure attached. This was simply to find out how much force it took to get the barge up to speed. Various runs were performed at differing velocities, with the results being recorded. The second trial involved the tripod structure attached to the top frame. This test allowed us to find out how much force it took to get the barge and the tripod up to speed. Again, various runs were performed at differing speeds.

Knowing that the line with the force transducer on it took the majority of the load from the barge when towing, but at a slight angle. Because of this, the true drag of the barge in the direction of travel would have to be calculated using vectors. While simple to do, it was not necessary because the true drag of the structure was simply the difference between the two runs.

Based on the recorded data during testing, a plot was created comparing the drag force both with and without the tripod structure attached to the frame. Because the data by itself could not yield an accurate drag calculation, parabolic best fit lines were added to both plots. The results of this comparison can be seen below in Fig. 33.

Knowing the equations of both best fit lines, as seen in Fig. 33, the overall drag of the structure could be gathered simply by taking the difference between these two equations for a variety of speeds. The overall drag results gathered for our tripod structure can be seen below in Fig. 34.

Theoretical calculations placed the overall drag of the tripod structure to be around 100 *lb.* at 6 *knots* ( $\approx 6 \text{ }^{feet}/_{sec}$ ). These theoretical calculations seem to follow the same trend as our experimental data showed. Thus we can confidently say the drag of the structure can be calculated using the best fit line data shown above in Fig. 33,34

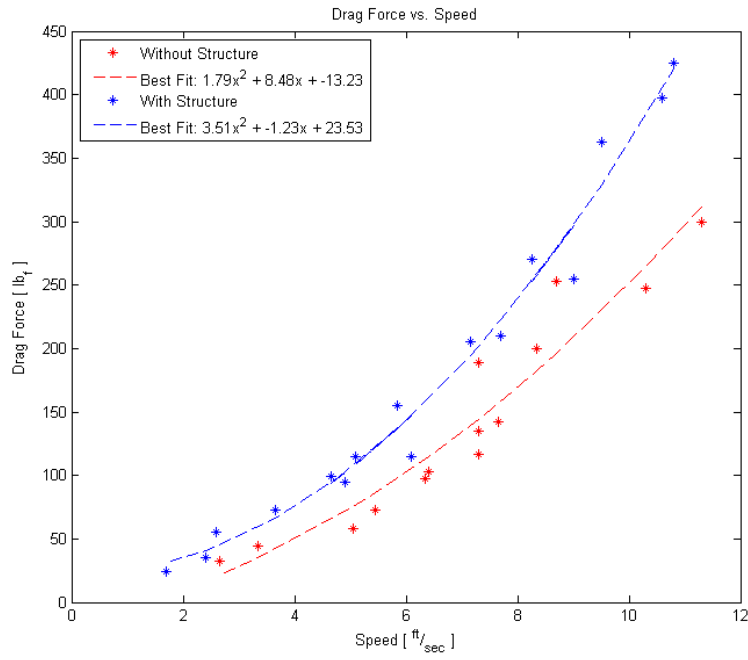


Figure 33: Initial drag data for both with and without the tripod attached

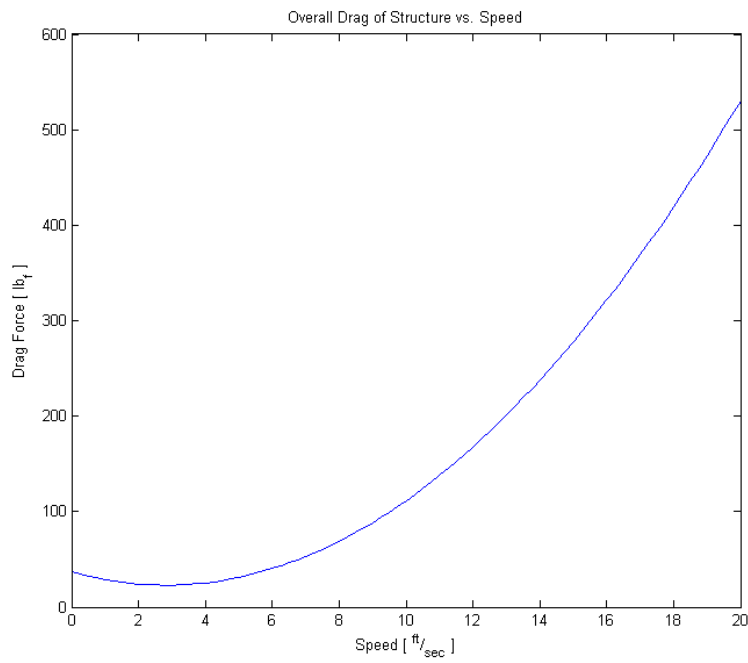


Figure 34: Overall drag of the structure compared to speed

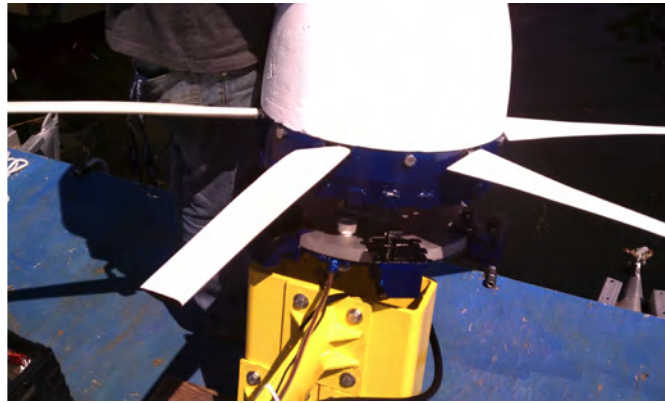


## 9.2 First Turbine Deployment

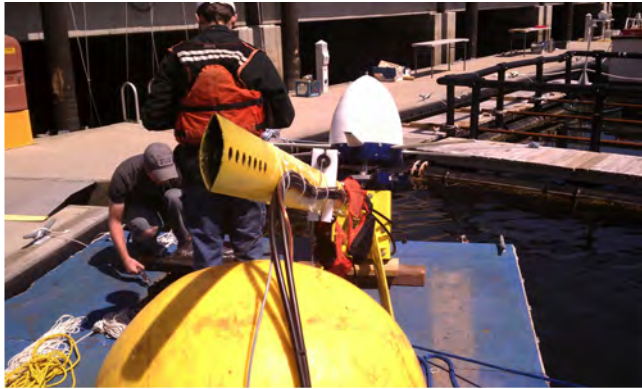
Though the structures design assured that the turbine could be mounted as planned, the turbine had never been attached to our structure. In order to prove the concept and prepare the assembly for future testing the full turbine assembly along with all the testing equipment was mounted to the support structure. Images and procedures are below.

- The turbine was carefully mounted by hand using eight 9/16 stainless steel bolts. The mounting configuration assures that the blades do not strike the structure, but that the turbine is close enough to the front airfoil to run up the various wires. See Fig. 35(a).
- Attached to the front airfoil is the copper wires used to carry the generated current of electricity, two hydraulic lines, the output to the laser tachometer, and the underwater camera wire. The underwater camera was mounted directly above the turbine and would be used to monitor the turbine and also be a back up to measure the turbines revolutions per minute. The ends of the wires were sent through a foam block and floated separately to assure they remained dry. See Fig. 35(b).
- The entire structure can be floated using either three 23 buoys or a single 4 buoy as shown. It was very important to have the turbine hang approximately 2 off the end of the barge before it was hoisted by the crane to assure that the blades were not damaged. Once lifted, the structure will hang with the turbines axis horizontally as planned, and it can be moved into the water. See Fig. 35(c).
- the floating structure is positioned under the barge and the hoisting cable is attached to the seamless ring below the buoy. Lifting it into place requires a minimum of four people with one person manning the capstan and the others positioning the structure.
- The first maneuver is to put a single 7/8 bolt through the front airfoil to alleviate its weight. Also, two 9/16 threaded rods are inserted into the L-bracket connectors to again alleviate the weight of the structure. Inserting the remaining bolts on the front airfoil and back plates proved difficult without the help of several people assisting and it is recommended that the holed be drilled to looser tolerances with the bolts in the future. At this point the buoys can be removed and testing can commence. See Fig. 35(d).

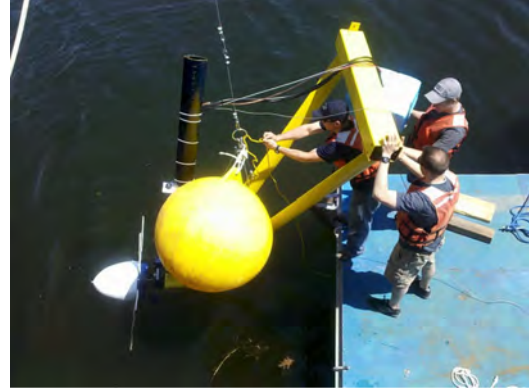
Due to restrictions on the towing boat use, the readiness of the turbine, and the weather, full testing was never accomplished this semester. Testing was scheduled to simply tow the barge with the full turbine attached, but our only available testing days were called off due to the weather and the lack of useful data that could be taken from the turbine at the time.



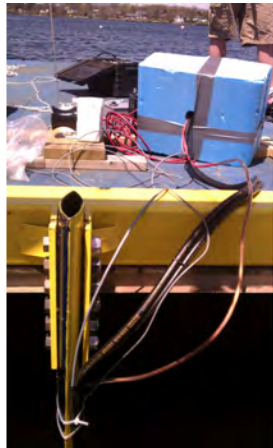
(a)



(b)



(c)



(d)

Figure 35: Cycle of pictures showing deployment procedures as described above



Figure 36: Image taken underwater of joint deployment

## 10 Future Work and Recommendations for Future Experiments

There is still much work to be done in future years to fine tune the deployment structure. The work performed by this years team successfully built off the ideas left behind by the previous team, and like them, have built solid building blocks upon which other groups can build from. Accurate testing of both this project, and it's sister group the VFG Turbine should be another year long project in and of itself. As a result, we strongly urge continued use of our projects.

While we addressed the major concern last years group had by streamlining the support structure with airfoils, our structure is still relatively heavy ( 360**lb**) and hard to transport. In future years, we would like to see an aluminum structure (provided calculations show its still strong enough to support foreseeable testing loads).

An aluminum structure would also solve the corrosion problem both our group and the last group faced. While we took every precaution we could to avoid corrosion (stainless-steel bolts, Rustoleum primer and paint on all steel surfaces), it still showed up. An aluminum structure would mean the structure wouldn't need to be painted (which can be toxic to marine life), and they could spend more time working on other facets. However, if aluminum ends up being either too pricey, or too weak, we recommend looking into power-coating the structure.

While the hip-tow we performed worked relatively well, future work should be done to secure and mount an engine on the barge itself. This would yield more options for testing, and more consistent data as the propeller blast would be behind the barge, not next to the barge.

A more efficient flotation system should be looked into. The buoys we used worked great, but they were always in the way, and a pain to deal with. In addition, the steel cables were always scratching the paint of of our front airfoil during deployment. If a system could be designed that allowed the structure to float on its own, that would eliminate a big hassle.

Lastly, while the capstan used during the deployment phase of our structure proved it could pull both the structure and tripod into position, it was at its very limit in terms of load bearing capabilities. Future tests should replace the capstan with something more suitable to heavy lifting such as a 12V Marine-Grade Winch.

## 11 Conclusion

The goal of this years VFG Support Structure was to create an ideal testing platform not only for the 2<sup>nd</sup> generation VFG turbine, but future horizontal axis turbines. Steps were taken to ensure the structure had a low drag coefficient, and was as easy to deploy as possible. The structural integrity was both analyzed rigorously and fabricated accurately providing confidence that the structure can perform high speed testing of turbines. The limitations of testing turbines inside Chase Hall will hopefully be mitigated using our structure. In the future, we hope it will help provide the 2<sup>nd</sup> generation VFG Turbine's group significantly more data to prove the VFG design concept.

## 12 Appendices

VFG DEPLOYMENT STRUCTURE: PRICE LIST

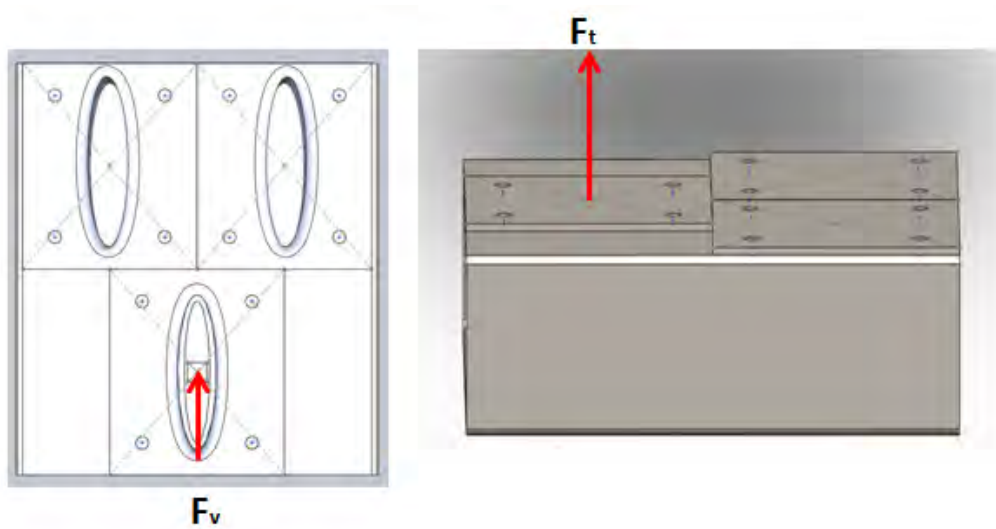
<u>SUPPLIER</u>	<u>ITEM</u>	<u>PRICE</u>	<u>REMAINING BUDGET</u>
			4000
<b>MONARCH INSTRUMENT</b>	Act-1B Tachometer		
	ROLS-W Remote Optical Laser Sensor		
	T-5WP Waterproof Reflective Tape		
	Shipping/Handling	580.80	
	SUBTOTAL	580.80	3419.20
<b>COLLINS SHEET METAL INC.</b>	(4) Front Strut Pieces		
	(4) Rear Strut Pieces		
	(5) 6.75" x 8" Attach Plates		
	Labor		
	SUBTOTAL	200.00	3219.20
<b>YARDE METALS</b>	(1) 6" x 6" x 0.25" Square Steel Tubing	163.00	
	(2) 4" x 4" x 0.25" Square Steel Tubing	140.00	
	(2) 6" x 8" x 0.25" x 16" Square Steel Tubing	150.00	
	(1) 6" x 8" x 0.25" x 51.5" Square Steel Tubing	156.00	
	(2) 5" x 14" x 0.5" Steel Plate	58.00	
	(4) 6" x 6" x 0.25" Steel Plate	60.00	
	(1) 6" x 14" x 0.5" x 16" Square Steel Tubing	248.00	
	SUBTOTAL	975.00	2244.20
<b>CUSTOM WELDING/FABRICATION INC.</b>	Air Foil Welding (One Full Days Work)	475.00	
	Remaining Welding	110.00	
	Waterjet Cutting	100.00	
	SUBTOTAL	685.00	1559.20
<b>McMASTER CARR INC.</b>	(1) 9/16" Drill Bit	33.25	
	(2) 9/16" High Speed Steel	44.07	
	(1) 9/16" Long Drill Bit	31.17	
	(1) 9/16" to 1" Step Drill Bit (\$55.90)	0.00	
	(1) 1" Cobalt Drill Bit	66.01	
	(1) 12"x12" SS Plate	18.05	
	(4) 2" SS Washers	15.08	
	Shipping	5.63	
	(1) 3' 7/16-13 Threaded Rod	9.41	
	Shipping	5.07	
	SUBTOTAL	227.74	1331.46
<b>FASTENER-WAREHOUSE.com</b>	(2) 72" long, 0.5" Diameter Threaded Stainles Rod	44.00	
	(7) 7/8" SS Bolts		
	(14) 7/8" Washers		
	(7) 7/8" Nuts	49.00	
	(8) 0.5" Diameter, 1.5" Length SS Bolts	8.40	
	(36) 0.5" Diameter Nuts	7.20	
	(96) 0.5" Diameter Washers	14.40	
	(12) 0.5" Diameter, 2" Length SS Bolts	10.80	
	(6) 3/16" Steel Cable		
	Seamless Ring		
	Rope Clips		
	U-Bolts		
	Caribbeaners	200.00	
	Locktite		
	Steel Cable	35.00	
	ESTIMATED SUBTOTAL	368.80	962.66
<b>Industrial Marine Supply</b>	Marine Foam (2 Qts)	38.94	
	SUBTOTAL	38.94	923.72
<b>Northeast Industrial Technologies</b>	Parts/Labor for Compound Angles/Holes	200.00	
	SUBTOTAL	200.00	723.72

**Home Depot**

(1) Rustolium Primer	30.59	
(1) Rustolium Paint	30.59	
(4) Paint Brushes	37.86	
(4) Sandpaper (400 + 800 grit orbital pads)	13.88	
(2) Tack Cloths	5.36	
(4) Paint Bins	8.56	
(1) 3-pack of wire brushes	3.47	
(1) Pack of towels	7.98	
	<b>SUBTOTAL</b>	<b>138.29</b>
		<b>585.43</b>

**Bicycle Bob's**

Mechanical Disk Brake Kit	49.99	
12' Steel Cable	12.99	
10' Cable Housing	14.99	
Brake lever	17.50	
	<b>SUBTOTAL</b>	<b>95.47</b>
		<b>489.96</b>



### Method:

The shear force on the bolted connection was first considered and the connection was defined to be a single-shear lap connection since the bolts had two surfaces of contact and one shear plane. From ASDM table I-D, the bolts used were ½ inch diameter, high-strength A325 designation, with slip critical condition. It was also assumed that there was Class A contact surface. From these assumptions, the allowable shear force  $f_v$  was found to be 17 ksi. The allowable shear load per bolt  $r_v$  was calculated using the equation

$$r_v = A_b * f_v$$

where  $A_b$  is the bolt cross-sectional area. The allowable shear load on the entire connection  $P_t$  is determined using the equation

$$P_t = r_v * n_b,$$

where  $n_b$  is the number of bolts in the connection. The allowable bearing stress  $F_p$  depends on the edge distance and center-to-center spacing of the bolts. From this it was determined that the bearing stress equation was

$$F_p = 1.2 * F_u ,$$

where  $F_u$  is the strength of the steel connecting plates (A36 steel assumed). The allowable bearing load per bolt is determined using

$$r_p = d * t * F_p ,$$

where  $d$  is the nominal bolt diameter and  $t$  is the thickness of the connecting plate. This was determined using table I-E in ASDM. The allowable bearing load per connection is finally determined using the equation

$$P_p = r_p * n_b .$$

The tension component of the bolted connection is determined by finding the allowable tension for one bolt. This is determined by

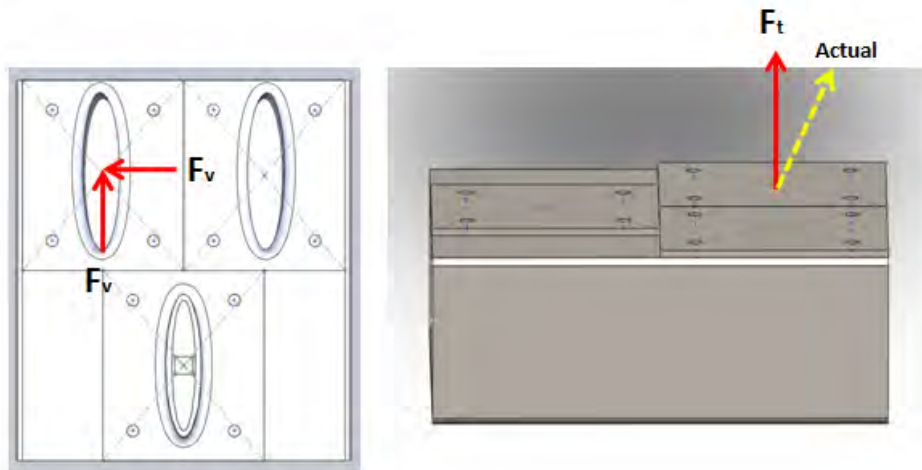
$$r_t = A_b * F_t$$

where  $F_t$  is determined from table 1-A in ASDM. Using A325 bolts  $F_t$  was found to be 44 ksi.  $r_t$  is compared to the actual tensional stress from the equation

$$F_t = \frac{P_t}{n_b A_b} .$$



Dimensions			Forces		
Number of Bolts	4	N/A	Bolt Shear Allowed	17	ksi
Bolt Diameter	0.5	in	Shear Force $f_v$	1.668	kips
Bolt Spacing	4	in	(Strength) $F_u$	58	ksi
Edge Distance	1	in	Tensile Force $f_t$	1.8	kips
Plate Thickness	0.25	in	Bolt Tension Allowed	44	ksi
<b>Allowable Shear Force/Bolt</b>					
Bolt CS-area	0.196	in <sup>2</sup>			
$r_v$	3.338	kips			
<b>Allowable Shear Force/Connection</b>					
$P_t$	13.352	kips			
<b>Actual shear Stress on Connection</b>			<b>Allowable Tension/Bolt</b>		
$F_v$	2.124	ksi	$r_t$	8.63937	kips
Factor of Safety	8.005	N/A	<b>Allowable Tension/Connection</b>		
			$P_t$	34.5575	kips
<b>Bearing</b>			<b>Actual Tensile Stress on Connection</b>		
Bearing Stress $F_p$	69.6	ksi	$F_t$	2.29183	ksi
Bearing Load $r_p$	8.7	kips	<b>Factor of safety</b>		
Bearing Load Connection $P_p$	34.8	kips	19.1986	N/A	



### Method:

First knowing the vector definition of the force, it can be broken into shear and tensile components. For the defined coordinate system, the force acting in both the x and the z vectors are combined to determine the net shear force on the bolt group. Again using ASDM table 1-D and A325 bolts the allowable bolt shear stress was found. The same method was used as in the front support to compare the allowable shear force to the actual shear force. To determine the allowable tensile stress in the bolts that are not in perfect tension, the following equation needs to be used

$$R_t = \sqrt{(44)^2 - 2.15(f_v)^2} .$$

This equation was determined from ASDM and is dependent on the bolt type (A325). This value is compared to the actual tensile stress determined using the equation

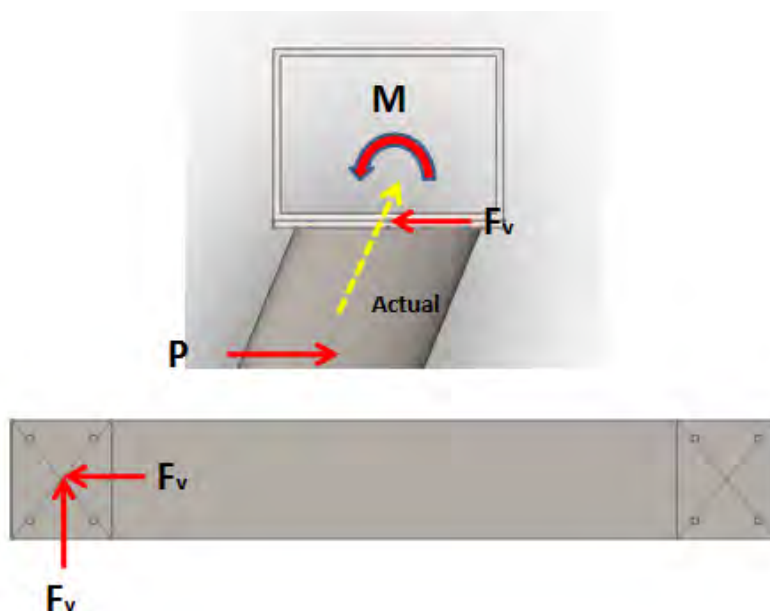
$$F_t = \frac{P_t}{n_b A_b} .$$

To test if the slip critical condition is acceptable to use, the actual tensile stress can be used to determine the allowable shear stress using the equation

$$F_v = 17.0 \left( 1 - \frac{f_t A_b}{T_b} \right) ,$$

where  $T_b$  is the minimum tension applied in the tightening process which was assumed to be 25 ksi. This value can be compared to the actual shear stress determined above.

Dimensions			Forces		
Number of Bolts	4	N/A	Bolt Shear Allowed	17	ksi
Bolt Diameter	0.5	in	Shear Force $f_{v,i}$	0.367	kips
Bolt Spacing	4	in	Shear Force $f_{v,k}$	0.161	kips
Edge Distance	1	in	(Strength) $F_u$	58	ksi
Plate Thickness	0.25	in	Tensile Force $f_t$	0.9	kilo-lbs
			<b>Allowable Bolt Tension</b>		
			Bolt Tension Allowed	43.9936	ksi
<b>Allowable Shear Force/Bolt</b>			<b>Allowable Tension/Bolt</b>		
Bolt CS-area	0.196	in <sup>2</sup>	$r_t$	8.63812	kips
$r_v$	3.338	kips			
<b>Allowable Shear Force/Connection</b>			<b>Allowable Tension/Connection</b>		
$P_t$	13.352	kips	$P_t$	34.5525	kips
<b>Actual shear Stress on Connection</b>			<b>Actual Tensile Stress on Connection</b>		
$f_v$ Actual (I and k)	0.40076	kips	$F_t$	1.14592	ksi
$F_v$	0.510	ksi	Factor of safety	38.3917	N/A
Factor of Safety	33.316	N/A			



### Method:

The force on the bottom of the leg can be translated to the centroid of the bolt group. Since the induced moment is about the x axis, it only induces a prying action. In the bolt group a neutral axis was chosen through the center of the connecting plate which puts two of the bolts in compression and the other two in tension. The neutral axis was defined by taking the vector sum of the shear components. The moment of inertia of the bolt group about the neutral axis was defined using the equation

$$I = \sum A_b d^2 .$$

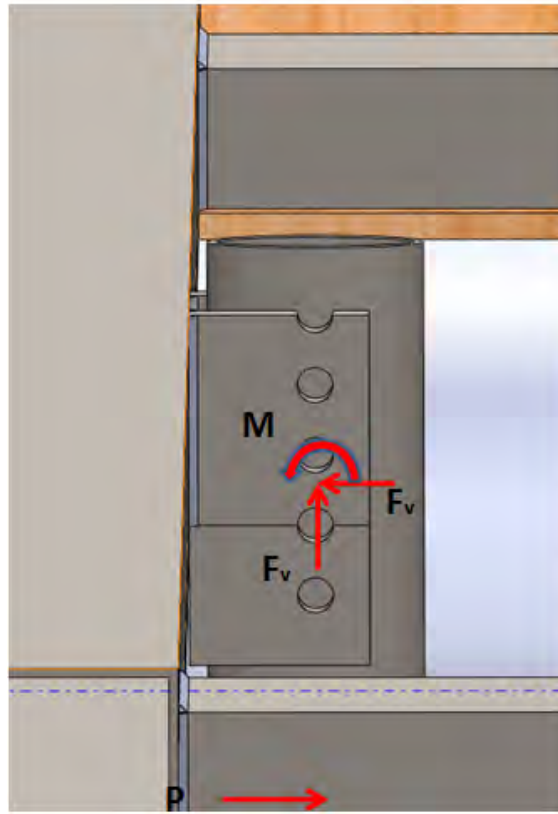
The actual tensile stress needs to be considered for the two bolts in tension. This can be determined using the equation

$$f_t = \frac{Pec}{I},$$

where  $Pe$  is the moment force and  $c$  is the distance from the bolt center to the neutral axis. The allowable shear force is computed as before and used to determine the allowable tensile stress using the equation

$$F_t = \sqrt{(44)^2 - 4.39(f_v)^2} .$$

Dimensions			Forces		
Number of Bolts	4	N/A	Bolt Shear Allowed	17	ksi
Bolt Diameter	0.5	in	Shear Force $f_{v,i}$	0.367	kips
Bolt Spacing	4	in	Shear Force $f_{v,k}$	0.161	kips
Edge Distance	1	in	(Strength) $F_u$	58	ksi
Plate Thickness	0.25	in			
Moment Arm (e)	106.00	in			
<b>Allowable Shear Force/Bolt</b>			<b>Allowable Bolt Tension</b>		
Bolt CS—area	0.196	in <sup>2</sup>	Bolt Tension Allowed	43.987	ksi
$r_v$	3.338	kips	<b>Moment Calculations</b>		
<b>Allowable Shear Force/Connection</b>			P	0.40076	kips
$P_t$	13.352	kips	$P*e$	42.4807	kips-in
<b>Actual shear Stress on Connection</b>			<b>Nuetral Axis Definition</b>		
$f_v$ Actual (I and k)	0.4007618	kips	Angle of Force Vector	0.41341	Degrees
$F_v$	0.510	ksi	Delta ( $A*\tan(\theta)$ )	0.87738	in
Factor of Safety	33.316	N/A	<b>Moment of Inertia about Nutral Axis</b>		
			$C_1$	3.87738	in
			$C_2$	2.12262	in
			$C_3$	2.12262	in
			$C_4$	3.87738	in
			$I_1$	2.95194	in <sup>4</sup>
			$I_2$	0.88465	in <sup>4</sup>
			$I_3$	0.88465	in <sup>4</sup>
			$I_4$	2.95194	in <sup>4</sup>
			I total	7.67318	in <sup>4</sup>
			<b>Actual Tensile Stress</b>		
			$F_{t1}$	21.4662	ksi
			$F_{t2}$	11.7514	ksi
			$F_{t3}$	11.7514	ksi
			$F_{t4}$	21.4662	ksi
			Factor of Safety	2.04913	N/A



### Method:

The vertical column of bolts makes up the bolt group which has a centroid between the two sets of bolts. Due to symmetry, it is assumed that the outer two bolts experience the largest shear forces, but the forces on each bolt will be analyzed. The polar moment of inertia  $I_{polar}$  is determined using the following equation

$$I_{polar} = \sum I_x + \sum I_y .$$

$I_x$  does not need to be considered for this scenario. The force in each component direction can be determined using the equation

$$f_t = \frac{Pec}{I} .$$

Since all the forces acting on the bolt are shear forces acting in many directions. All the forces need to be added vectorally to find the net shear force and determine if it is less than the allowable shear force of the bolts.

Initially with only 4 bolts, the shear stress exceeded the bolt strength. With 6 bolts however, the bolt shear forces decreased dramatically, however, one bolt theoretically will still yield.

Dimensions			Forces		
Bolt Diameter	1	in	$F_{front,j}$	1.8	kips
L_bolt	2	in	$F_{front,i}$	1.668	kips
Bolt Radius	0.5	in	Bolt Shear Allowed	17	ksi
L_beam	113.5	in			
CS_area_bolt	0.7853975	in <sup>2</sup>			
Number_Bolts	6	N/A			

Force Components Stress				
Bolt	Fx_per_bolt		Fy_per_bolt	
A	-0.353960892	ksi	-0.381972186	ksi
B	-0.353960892	ksi	-0.381972186	ksi
C	-0.353960892	ksi	-0.381972186	ksi
D	-0.353960892	ksi	-0.381972186	ksi
E	-0.353960892	ksi	-0.381972186	ksi
F	-0.353960892	ksi	-0.381972186	ksi
Allowable/Bolt	13.3517575	kips		

Geometry				Moment Force	
Bolt	Cy	Cx		M	189.318 kips-in
A	3	in	0		
B	1	in	0		
C	-1	in	0		
D	-3	in	0		
E	5	in	0		
F	-5	in	0		

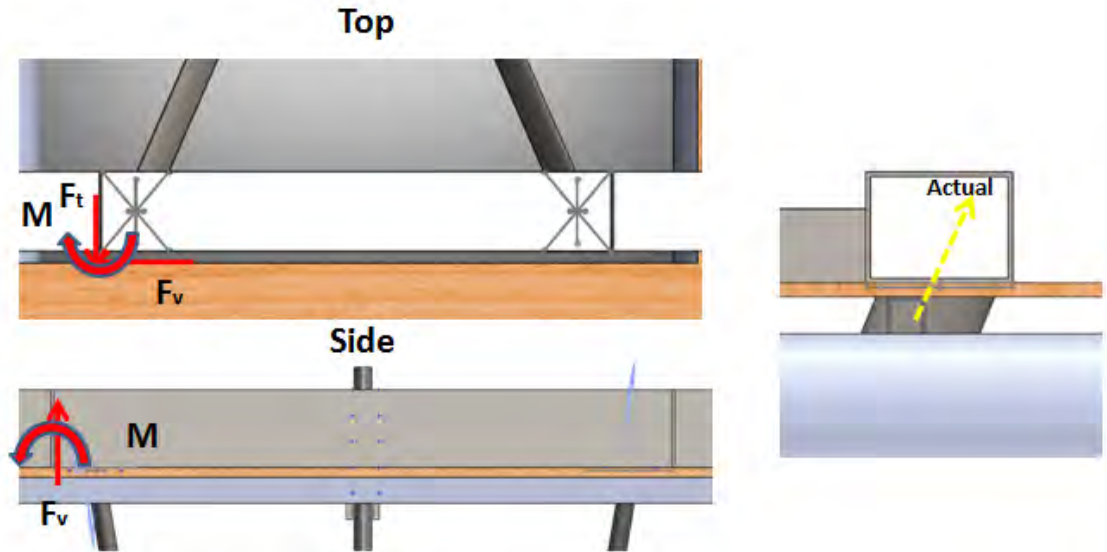
Moment of Inertia				
Bolt	Ix	Iy		
A	7.0685775	in <sup>4</sup>	0	in <sup>4</sup>
B	0.7853975	in <sup>4</sup>	0	in <sup>4</sup>
C	0.7853975	in <sup>4</sup>	0	in <sup>4</sup>
D	7.0685775	in <sup>4</sup>	0	in <sup>4</sup>
E	19.6349375	in <sup>4</sup>	0	in <sup>4</sup>
F	19.6349375	in <sup>4</sup>	0	in <sup>4</sup>
		$I_p$	54.977825	in <sup>4</sup>

Moment Forces				
Bolt	Fmx_per_bolt	Fmy_per_bolt		
A	10.33060147	ksi	0	ksi
B	3.443533825	ksi	0	ksi
C	-3.443533825	ksi	0	ksi
D	-10.33060147	ksi	0	ksi
E	17.21766912	ksi	0	ksi
F	-17.21766912	ksi	0	ksi

Resultant Forces							
Bolt	Fx	Fy	F	Factor of Safety			
A	9.976640582	ksi	-0.381972186	ksi	9.98395	ksi	1.70273
B	3.089572932	ksi	-0.381972186	ksi	3.1131	ksi	5.4608
C	-3.797494717	ksi	-0.381972186	ksi	3.81666	ksi	4.45416
D	-10.68456237	ksi	-0.381972186	ksi	10.6914	ksi	1.59006
E	16.86370823	ksi	-0.381972186	ksi	16.868	ksi	1.00782
F	-17.57163002	ksi	-0.381972186	ksi	17.5758	ksi	0.96724



### Method:

The force in the x direction induced both tension on the bolt group and a prying moment that puts half the bolts in tension and the other in compression about the neutral axis. Next, the force in the z direction has uniform shear on the bolts and does not induce a moment. Lastly, the force in the y direction induces uniform shear in the bolt and a moment that induces more shear forces on the bolt and can be determined using the principles of eccentricity. Both the second moment of area of the bolt group and the polar moment of inertia are needed for this analysis. This method is slightly different than the previous analysis. To find the allowable tension force based on the shear force on the bolt the equation

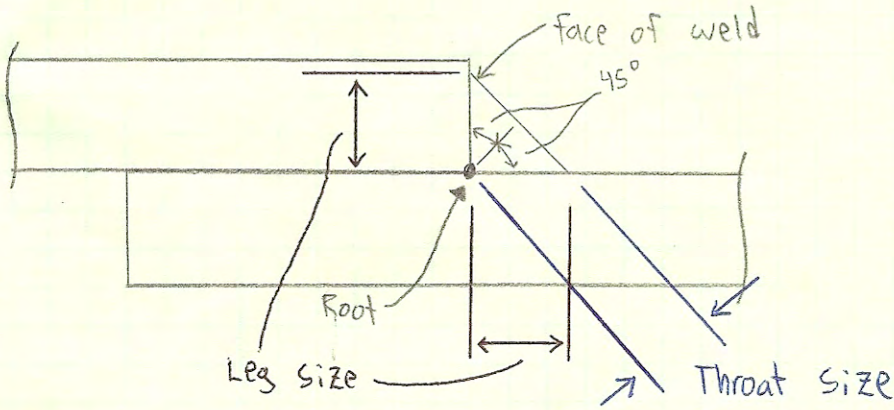
$$F_t = \sqrt{(44)^2 - 4.39(f_v)^2}$$


is needed. Both the shear and the tension in the bolts are compared to the allowable shear and tensile stress allowed for the bolts.

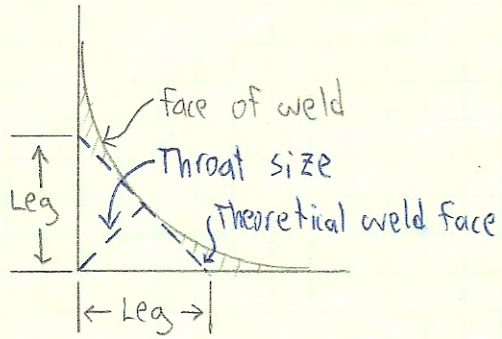


Dimensions			Forces		
Number of Bolts	4	N/A	Bolt Shear Allowed	17	ksi
Bolt Diameter	0.75	in	Force $f_{v,i}$	0.367	kips
Bolt Spacing	3	in	Force $f_{v,k}$	0.161	kips
Edge Distance	1.5	in	Force $f_{v,j}$	0.899	kips
Plate Thickness	0.25	in	(Strength) $F_u$	58	ksi
Moment Arm about Y	3.56	in			
Moment Arm about X	3.56	in			
Allowable Shear Force/Bolt			Moment Forces		
Bolt CS—area	0.442	in <sup>2</sup>	About Y	1.30652 kips—in	
$r_v$	7.510	kips	About X	3.20044 kips—in	
Moment About Y and X			Shear Force from Force in k Direction		
$C_1$	1.5	in	$F_{v,1,k}$	0.04025 kips	
$C_2$	1.5	in	$F_{v,2,k}$	0.04025 kips	
$C_3$	1.5	in	$F_{v,3,k}$	0.04025 kips	
$C_4$	1.5	in	$F_{v,4,k}$	0.04025 kips	
$I_1$	0.99402	in <sup>4</sup>			
$I_2$	0.99402	in <sup>4</sup>	Shear Force from Force in Y Direction		
$I_3$	0.99402	in <sup>4</sup>	$F_{v,1,y}$	0.25253 kips	
$I_4$	0.99402	in <sup>4</sup>	$F_{v,2,y}$	0.25253 kips	
I total	3.97607	in <sup>4</sup>	$F_{v,3,y}$	0.25253 kips	
			$F_{v,4,y}$	0.25253 kips	
Tension Force from Moment about Y			Shear Force from Moment about X		
$F_{t,1}$	0.49289	ksi	Sum( $I_{zz}$ )	9	in <sup>2</sup>
$F_{t,3}$	0.49289	ksi	Sum( $I_{y2}$ )	9	in <sup>2</sup>
Pure Tension/bolt			I Polar (J/A)	18	in <sup>2</sup>
$F_t$	0.20768	ksi	C bolts	2.12132	in
Allowable Tensional Force (calculated)			$Q_{mu}$	0.1778	kips/in
ft	43.5899	ksi	$Q_m$	0.37718	kips
Totals			$F_{mk}$	0.2667	kips
$F_{t,1}$	0.70057	ksi	$F_{my}$	0.2667	kips
$F_{t,2}$	0.20768	ksi	Total Shear Force on Each bolt		
$F_{t,3}$	0.70057	ksi	$F_{v,1}$	1.36531 ksi	
$F_{t,4}$	0.20768	ksi	$F_{v,2}$	1.36531 ksi	
Factor Of Safety	62.2203	N/A	$F_{v,3}$	1.36531 ksi	
			$F_{v,4}$	1.36531 ksi	
			Factor of Safety	12.4514 N/A	

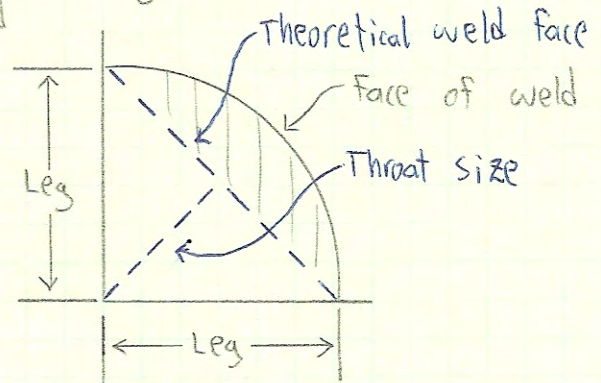
Typical Fillet weld



assume that  = doesn't add strength to weld

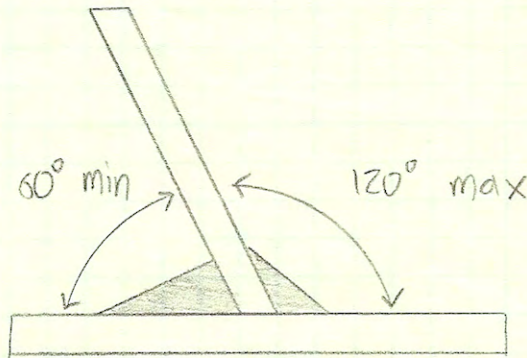


(a) concave



(b) convex

\* convex is more desirable b/c less prone to cracking as a result of the shrinking during cooling



note: leg length must be > 1/4" Per ASDS Regs.

Skewed Fillet weld limitations

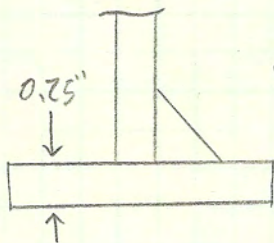
\* welds outside of these limits, considered to be groove welds

\* Fillet welds are stronger in tension/compression than shear, the controlling fillet weld stresses considered to be shear stresses on effective throat area

\* Throat area establishes strength of fillet weld.

with equal leg sizes

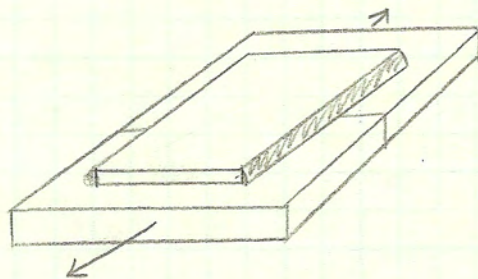
$$\text{effective throat distance} = \sin(45^\circ) \cdot \text{leg-size}$$



$$\text{eff. throat dist.} = (0.707)(0.25) = \boxed{0.17675''}$$

approx 3/16" rounding up

\* assume loaded parallel per ASDS (Table J2.5) standards



$$F_v = 0.3 F_u$$

$F_v$  = allowable shear stress

$F_u$  = specified min tensile strength of electrode

$$P = F_u (\sin(45^\circ)) (\text{leg-size}) (0.3) \text{ where } P = \text{strength fillet weld per linear inch}$$

\* most widely used electrode = E70 which is compatible with all grades of steel up to  $\sigma_{T_s} = 60 \text{ ksi}$

$$E70XX \rightarrow F_u = 60 \text{ ksi}$$

$$P = (0.3)(60 \text{ ksi})(0.707)\left(\frac{1}{4}\right) = \boxed{3.14 \frac{\text{KIPS}}{\text{inch}}}$$

note: for shielded metal arc welding

$$\text{weld capacity} = (P)(L_{\text{weld}}) \quad \left\{ \begin{array}{l} (2)(3.14)(6.75'') = 42.93 \\ (2)(3.14)(4'') = 50.48 \end{array} \right\} \boxed{93.41 \text{ KIPS}}$$

block shear strength

$$P_t = A_v F_v + A_t F_t = A_v (0.30 F_u)^{160 \text{ ksi}} + A_t (0.5 F_u)^{60 \text{ ksi}}$$

$A_v$  = net shear area

$A_t$  = net tension area

⇒ allowable tensile load per side:

$$P_t = A_v (0.3 F_u)^{160 \text{ ksi}} = ((6.75)(0.25))((0.3)(60 \text{ ksi}))$$

$$P_t = 30.375 \text{ ksi}$$

⇒ allowable shear load per side:

$$P_t = A_t (0.5 F_u)^{60 \text{ ksi}} = (8 \cdot 0.25)(0.5 \cdot 60)$$

$$P_t = 60 \text{ ksi}$$

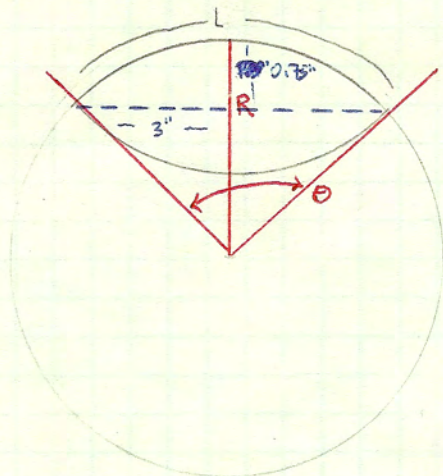
⇒ total block shear strength

$$P_t = 2(30.375) + 2(60)$$

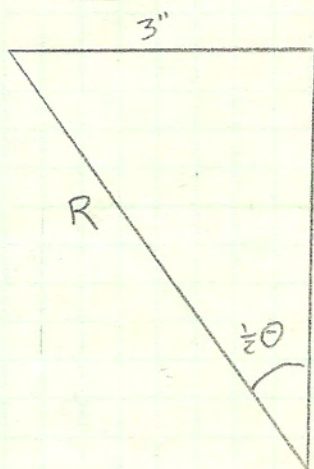
$$P_t \text{ total capacity} = 140.75 \text{ ksi}$$

note

need circumference of ellipses

Airfoil Circumference Calculations

$$L = \overset{\text{radians}}{\theta} r = \frac{\overset{\text{degrees}}{\alpha} \pi r}{180}$$



$$\sin\left(\frac{1}{2}\theta\right) = \frac{3}{R} \rightarrow R \sin\left(\frac{1}{2}\theta\right) = 3 \quad \textcircled{1}$$

$$R - 0.75 = \cos\left(\frac{1}{2}\theta\right) \cdot \frac{R - 0.75}{R} \rightarrow R \cos\left(\frac{1}{2}\theta\right) = R - 0.75 \quad \textcircled{2}$$

$$\textcircled{1} \quad R = \frac{3}{\sin\left(\frac{1}{2}\theta\right)}$$

$$\textcircled{2} \quad \left(\frac{3}{\sin\left(\frac{1}{2}\theta\right)}\right) \cos\left(\frac{1}{2}\theta\right) = \left(\frac{3}{\sin\left(\frac{1}{2}\theta\right)}\right) - 0.75$$

$$\hookrightarrow \theta = 56.145^\circ = 0.979915 \text{ radians}$$

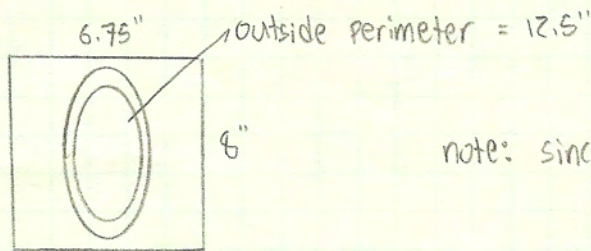
$$R = \frac{3}{\sin\left(\frac{1}{2}\theta\right)} \rightarrow R = 6.375''$$

$$L = R\theta \rightarrow L = (6.375'')(0.979915 \text{ rad}) = 6.24696''$$

Total Perimeter

$$P = 2L \rightarrow P_{\text{total}} \approx 12.5''$$

for bottom plates/struts



note: since tensile area approaches 0, only shear load will be considered

$$\text{block shear strength, } P_t = A_v F_v + A_t F_t = A_v (\cancel{0.30 F_u}) + A_t (0.5 \cancel{F_u}) \quad \begin{matrix} \nearrow 60 \text{ ksi} \\ \nearrow 60 \text{ ksi} \end{matrix}$$

→ allowable shear load per circumference:

$$P_t = A_t (0.5 F_u) = (12.5 \cdot 0.25) (0.5 \cdot 60 \text{ ksi})$$

$$P_t = 93.75 \text{ ksi}$$

$$\text{total capacity} = 93.75 \text{ ksi}$$

for top plates/struts

knowing width increased to 6.5" from 6", (approximate)

Perimeter weld  $\approx 14$ "

$$\text{total capacity} = 105 \text{ ksi}$$

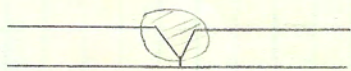
\* however, if combined with welding of plate

$$\text{total capacity} = 160.75 + 105 = 265.75 \text{ ksi}$$

\*\* note: 1 ksi = 1000 psi = Force \*\*

Groove weld b/w two airfoil sections

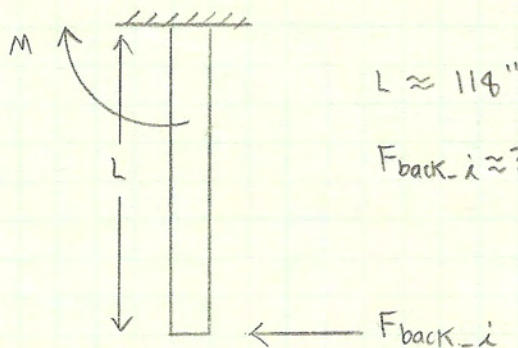
note: assume vee-groove pattern



→ if proper electrode is used w/ parent metals, allowable stresses in the weld will be same as parent material

moment at top attach plates

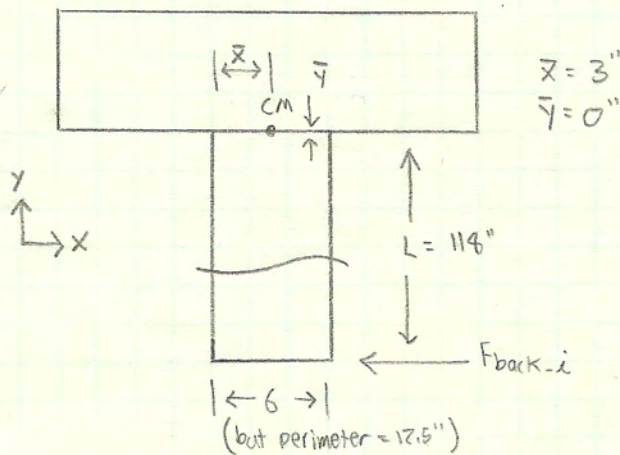
note, assumed straight cantilever beam welded eccentrically



$$L \approx 114''$$

$$F_{back-i} \approx 364 \text{ lbf} \quad (\text{from bolt calculations})$$

$$M = (F_{back-i})(L) = (364 \text{ lbf})\left(\frac{114''}{12''}\right) = \boxed{3619 \text{ lb-ft}}$$



$$J = I_x + I_y$$

$$I_y = \frac{1}{12}(12.5'')^3 + (12.5)(3'')^2 = 275.26 \text{ in}^2$$

$$I_x = \frac{1}{12}(6'')^3 + 0 = 0 \text{ in}^2$$

$$\boxed{J = 275.26 \text{ in}^2}$$

$$\text{torsional moment, } M = (364 \text{ lbf})(114'') = 43.424 \text{ in-kips}$$

$$\text{force on weld due to moment, } P_m = \frac{M r}{J}$$

where  $r$  = greatest dist. from weld center = 3"

$$P_m = \frac{(43.424)(3'')}{275.26} = \boxed{0.4733 \text{ kips/in}}$$

$$\rightarrow \text{total force from } M = (P_m)(12.5) = \boxed{5.9163 \text{ kips}}$$

Weld Capacity (using Fillet welds)

$$P = F_u (\sin(45^\circ)) (\text{leg size}) (0.3) \quad \text{where } P = \text{strength weld/in}$$

$F_u = \text{min tensile strength of electrode}$

→ assuming E70 electrode,  $\sigma_{ys} = 60 \text{ ksi}$   
 $F_u = 60 \text{ ksi}$

$$P = (0.3)(60 \text{ ksi})(0.707)(\frac{1}{4} \text{''})$$

$$P = 3.14 \text{ kips/in}$$

$$\text{weld Capacity} = (P)(L\text{-weld}) = (3.14)(12.5 \text{''}) = 39.75 \text{ kips}$$

Factor of safety

$$FS = \frac{\text{Weld Capacity}}{\text{Weld Load}} = \frac{39.75 \text{ kips}}{5.9163 \text{ kips}}$$

$$FS = 6.714$$

Reference

Applied structural steel Design - 3rd edition

↳ Leonard Spiegel

↳ George F. Limbrunner



# Buoyancy Free Body Diagrams

- 5 attach Plates → 18.9 lb
- 2 rear struts → 94.14 lb
- 1 Front strut → 45.69 lb
- 1 middle frame → 98.47 lb
- 1 box → 86.1 lb

Solidworks =

marine foam =  $60 \left( \frac{\text{lb}_f}{\text{ft}^3} \right)$

✓ Front strut =  $0.2974 \text{ ft}^3$

✓ Rear strut =  $0.3098 \text{ ft}^3$

✓ Frame =  $0.943 \text{ ft}^3$

## Buoyancy

$F = 17.644 \text{ lb}_f$

$R = 18.5475 \text{ lb}_f$  (each)

Frame =  $56.56 \text{ lb}_f$

